Modeling of Rock Failure Under PDC Cutter Based on Lab Experiments

by

Vivek K Prajapati, B. Tech

A Thesis

In

PETROLEUM ENGINEERING

Submitted to the Graduate Faculty
of Texas Tech University in
Partial Fulfillment of
the Requirements for
the Degree of

MASTER OF SCIENCE

in

PETROLEUM ENGINEERING

Approved

Dr. Malgorzata Ziaja
Committee Chair

Dr. Marshall Watson

Dr. Waylon House

Peggy Gordan Miller
Interim Dean of the Graduate School

May, 2011

Dedication

This work is dedicated to my loving parents.

ACKNOWLEDGMENTS

I take this opportunity to thank each and every person who has helped me in some way or the other for the successful completion of my Master's thesis research.

First, I would like to thank Dr. Malgorzata Ziaja, my thesis advisor, for all the help and the timely guidance that she provided. I thank her for all the time that she spent mentoring me. I truly learned a lot under her mentorship and I am always grateful to her.

I would also like to thank my other committee members, including Dr. Marshall Watson and Dr. Waylon House. I would also like to acknowledge Paul Lutes of Baker Hughes, who was instrumental in providing me the rock samples required for the experiments. I would also like to thank Joe McInerney for his immense help in conducting my experiments.

I would like to thank my friends, for their constant encouragement and mental support. Without their presence, my success wouldn't have been possible. Finally, I would like to thank my parents for their continued love and support.

TABLE OF CONTENTS

ACKNOWLEDGMENTS ii

ABSTRACT v

LIST OF FIGURES vi

CHAPTERS

I. INTRODUCTION 1

II. CHIP FORMATION IN THE CUTTING PROCESS 7

2.1 Literature Review 7

2.2 Models of Rock Cutting 24

2.3 Discussion on Single Shear Plane Models 36

III. ROCK DRILLABILITY 38

3.1 Rock Mechanical Properties 38

3.2 Failure Criterion in Rocks 41

3.3 Factors Affecting Failure of Rock 46

3.4 Effect of Bottomhole Pressure Conditions on Drilling 55

IV. SPECIFIC ENERGY IN DRILLING 63

4.1 Properties Used as Drillability Index 63

4.2 Mechanical Specific Energy 66

4.3 Literature Review 69

4.4 Expressions of MSE 74

4.5 Industry Application of MSE 75

V. EXPERIMENTAL SET UP 81

5.1 MICROBIT Simulator 81

5.2 MICROBIT User Interface 87

5.3 Rock Samples and Properties of Rock Sample 90

5.4 Steps Followed During the Experiments 91

VI. RESULTS AND DISCUSSIONS 94

VII. CONCLUSIONS 119

VIII. RECOMMENDATIONS FOR FUTURE WORK 121

REFERENCES 123

ABSTRACT

In the petroleum industry, drilling is one of the most important aspects due to the economics. Reduction in drilling time is encouraged to minimize the cost of operations. The choice of drilling bits becomes critical to maximize the rate of penetration and minimize the tripping time, thereby decreasing the cost of operations.

Mechanical specific energy is being used as a new trending tool to optimize the drilling process because of its sensitivity to all the basic parameters of the drilling process. It can be used to help us identify bit balling, bottomhole balling, excessive vibrations, and bit dulling. Due to a better understanding of the bottomhole conditions and a proactive approach to correcting any inefficient parameters, it is encouraged to use mechanical specific energy as a drilling process efficiency indicator on the rig site.

In this study, a set of laboratory drilling tests have been carried out on Carthage Marble and Crab Orchard at different confining pressures. A high pressure simulator is used to simulate different bottomhole conditions. Mechanical specific energy variation at different pressures has been analyzed. It is concluded that as the pressure increases, mechanical specific energy increases and that as the depth of cut increases, mechanical specific energy decreases.

LIST OF FIGURES

1.1. Parameters defining bit geometry 5
2.1. Orthogonal model of cutting in metals..... 8
2.2. Diagram of rock failure 9
2.3. Models of rock cutting mechanism for (a) diabase and (b) granite . 12
2.4. Failure mechanism 14
2.5. Deformation zones in orthogonal cutting..... 15
2.6. Failure process of rock cutting..... 17
2.7. Schematic of metal plate deformation..... 17
2.8. Chip formation in cutting natural brittle materials 18
2.9. Chip formation (a) without confining pressure and (b) with confining pressure..... 19
2.10. Lip schematic in soft and hard formation 22
2.11. Merchant model of cutting 25
2.12. Evans model of cutting 29
2.13. The stress and cutting forces for rock cutting..... 31
3.1. Common laboratory schematic for unconfined compression test.. 39
3.2. Common laboratory schematic for triaxial compression test 40
3.3. The Mohr-Coulomb failure criterion 42
3.4. Failure behavior of a South African slate..... 50
3.5. Influence of mean stress on the ductile/brittle transition of Carrare Marble..... 52
3.6. Influence of temperature on the behavior of granite..... 54
5.1. Schematic of drilling experiment set up..... 85
5.2. Schematic of rock holder..... 86
5.3. User interface of MICROBIT program 88
6.1. Change in specific energy with depth for Carthage Marble at different pressures 95
6.2. Change in specific energy with depth for Crab Orchard at different pressures 96
6.3. Change in specific energy with DOC for Carthage Marble at different pressures 97
6.4. Change in specific energy with DOC for Crab Orchard at different pressures 99
6.5. Specific energy vs. depth for Carthage Marble and Crab Orchard at 250 psi..... 100
6.6. Specific energy vs. depth for Carthage Marble and Crab Orchard at 500 psi..... 100
6.7. Specific energy vs. depth for Carthage Marble and Crab Orchard at 1,000 psi..... 101

6.8. Specific energy vs. DOC for Carthage Marble and Crab Orchard at 250 psi 102
6.9. Specific energy vs. DOC for Carthage Marble and Crab Orchard at 500 psi 102
6.10. Specific energy vs. DOC for Carthage Marble and Crab Orchard at 1,000 psi 103
6.11. ROP vs. DOC for Carthage Marble at different pressures 103
6.12. ROP vs. DOC for Crab Orchard at different pressures 104
6.13. ROP vs. DOC for Carthage Marble and Crab Orchard at 250 psi 105
6.14. ROP vs. DOC for Carthage Marble and Crab Orchard at 500 psi 105
6.15. ROP vs. DOC for Carthage Marble and Crab Orchard at 1,000 psi 106
6.16. Cutting force vs. DOC for Carthage Marble at different pressure 107
6.17. Cutting force vs. DOC for Crab Orchard at different pressure ... 108
6.18. Cutting force vs. DOC for Carthage Marble and Crab Orchard at 250 psi 109
6.19. Cutting force vs. DOC for Carthage Marble and Crab Orchard at 500 psi 109
6.20. Cutting force vs. DOC for Carthage Marble and Crab Orchard at 1,000 psi 110
6.21. Change in porosity with DOC in Carthage Marble at different confining pressures 111
6.22. Change in porosity with DOC in Crab Orchard at different confining pressures 111
6.23. Grains shown in a thin section of Carthage Marble 113
6.24. A large size grain as seen in a thin section of Carthage Marble . 114
6.25. Grains shown in a thin section of Crab Orchard 115
6.26. Grains in the cuttings obtained from the drilling experiments .. 116
6.27. Grains in the cuttings obtained from the drilling experiments in a different position 116
6.28. Grains in the cuttings obtained from the drilling experiments in a different position in a different view 117

CHAPTER I

INTRODUCTION

Rock drilling is a primary activity in the oil, mining, and construction industries. The method of drilling depends on various parameters such as rock properties, equipment availability, and the specific requirements of a particular well. The basic tool used in drilling is a drill bit. In certain geological conditions, the selection of the correct drill bit to reduce the cost of operation is the most challenging problem. At present, a large variety of bits are available for different conditions, so it is important to choose a bit that is needed to fulfill a specific requirement. Selection of the correct bit results in higher penetration rate and minimum wear of the bit during drilling, which constitutes an economical drilling operation.

Rock drilling technology saw a major breakthrough in the early 1970s because of the introduction of polycrystalline diamond compacts (PDC) as cutting elements. The introduction of PDC cutters allowed the rocks to be sheared rather than being crushed, which resulted in a significant increase in the rate of penetration during drilling. The rate of penetration during drilling is increased because the shear strength is less than the compressive strength of the rock. PDC bits are designed to give a certain penetration per revolution by carefully selecting the size and the number

of PDC blanks. The length of the cutters projected from the face of the bit is used to define the bottom clearance, which helps in efficient removal of cutting from the bottom.

While introduction of PDC cutters meant the use of fewer bits, fewer trips to change the dull bits, and hence a significant savings in the overall cost of drilling; their failure in hard rocks was also emphasized. Because of their low durability in hard rocks, the application of PDC cutters was limited to the soft, firm and medium hard, non-abrasive rocks.

Feenstra [1] reported that low durability of PDC bits was due to their high temperature instability and low impact resistance in the hard rocks. This low durability was also because of the poor bit selection criterion, bit design, and lack of understanding of the rock/bit interaction process.

Also, problems of bit balling in very soft and gummy formations, breakage and premature cutter abrasion in the hard and abrasive formations have been frequently reported for the PDC bits and were a serious cause of concern among drilling operators. However, due to recent developments in the bit metallurgy, PDC bits are now used more frequently.

Due to these reasons, the PDC cutters have always attracted a great deal of attention from researchers. Again, due to the high cost of experimentation and general difficulty in observing the material removal

process, numerical simulation tools have found their way into the research.

Three approaches of modeling the rock/bit interaction [2] are as follows:

Field or Laboratory Test: Under various required/desired operating conditions, actual field or laboratory tests are carried out for a full bit and a single PDC cutter. Generally, bits and cutters are armed with measuring devices such as strain gauges to collect the magnitudes of axial, tangential, and radial drilling forces acting on a full bit or a single cutter. Many times, researchers use actual field or laboratory data to develop the empirical correlations based on the curve fitting.

Analytical Approach: Researchers have put in a lot of effort into developing full bit models that are based on the single cutter analytical models. These models predict forces acting on a single cutter and the friction between the rock and the cutting face/edge of the PDC cutter. These models consider complex bit geometry and cutter orientation to predict the desired drilling parameters.

Numerical Modeling Approach: Numerical models depicting the single cutter/rock interaction have been developed and are used to predict the stress state in rock mass, forces, and the thermal response generated during the process. These models use the continuum based finite

element, finite difference method, or the discrete element method to model the rock/bit interaction.

PDC Bit

PDC bits [3] use drill blank as a cutter element. These cutter elements are made of two basic components: a layer of synthetic polycrystalline diamonds and a tungsten carbide layer. This layer of synthetic polycrystalline diamonds is sintered under high pressure and temperature to the top of the tungsten carbide layer. Also, the tungsten carbide layer can be in the form of a tungsten carbide bit-body matrix or a tungsten carbide stud.

There are several important geometrical design parameters that are used to describe a particular bit. These parameters define the orientation of the cutter on the bit: back rake angle, side rake angle, and the cutter exposure or chip clearance. Back rake angle is a measure of the aggressiveness of the cutter on the bit. A smaller back rake angle is favored in soft and nonabrasive formations to increase the aggressiveness due to the low cutter wear. Side rake angle is helpful in pushing the cuttings to the side of the hole. The cutter exposure, or chip clearance is defined as the amount of PDC face that is exposed to the rock. **Fig. 1.1** demonstrates these parameters in two dimensions.

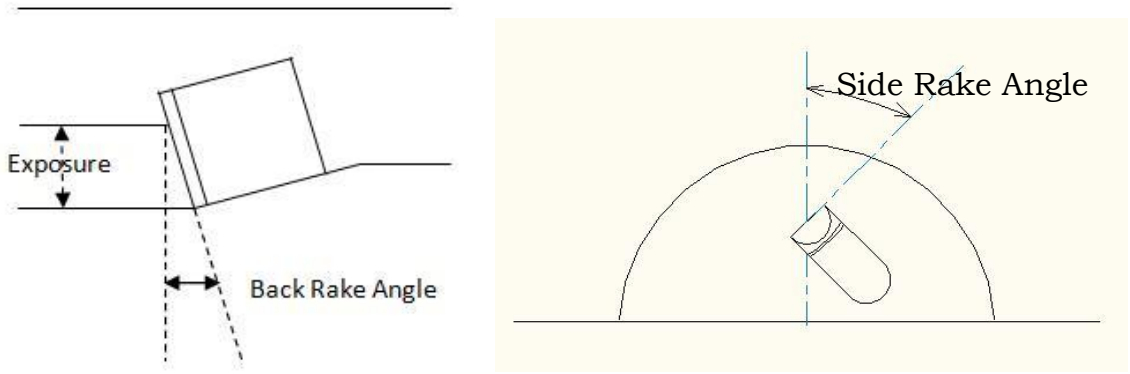

Fig. 1.1: Parameters defining bit geometry [3]

Other design parameters include the size, shape, and number of cutters.

In the past, different rock parameters have been used as bit selection criterion for particular formations like hardness, unconfined compressive strength (UCS), and confined compressive strength (CCS). Studies have correlated the drilling efficiency with the known rock properties. All drilling environments have an inherent degree of difficulty that is only associated to that location or well. Mechanical specific energy (MSE) is one parameter that depends on rock properties, bit design, drilling parameters, and bottomhole conditions. Recent studies have shown that MSE can be used as a trending parameter to optimize the efficiency of drilling operations.

The objective of this study is to investigate the effect of confining pressure on the process of rock failure and the drilling specific energy experimentally. High pressure drilling equipment will be used to conduct drilling experiments on Carthage Marble and Crab Orchard. Carthage

Marble and Crab Orchard are selected for the experiments because of vast difference in their unconfined compressive strength.

Efforts will be made to relate the effect of the confining pressure on the depth of cut for effective drilling. Specific energy, rate of penetration, and cutting force are to be analyzed at different pressures. Drilling parameters of Carthage Marble and Crab Orchard are to be compared with varying confining pressures.

These experiments under different pressure conditions will provide invaluable information to the industry for micro-bit operations. The effect of pressure on the drilling response of two rock types will give a good insight on the drilling process.

CHAPTER II

CHIP FORMATION IN THE CUTTING PROCESS

Researchers acknowledge that the removal of material during rock drilling can be grouped into three types. Depending on the type of the bit used in the drilling process, it can be classified as indentation (crushing), cutting (shearing), or scraping (abrasion). Roller bits are designated to use an indentation mechanism to crush the rock while PDC bits employ a cutting mechanism to shear the rock. Surface set and impregnated diamond bits drill rocks by abrasion.

2.1 Literature Review

Olson et al. [4] in their analysis of chip dynamics in metal cutting gave a good insight into the orthogonal model of cutting **(Fig. 2.1).** In metals, the tangential velocity of the chip is taken proportional to the cutting velocity since the cutting process is considered an isochoric (volume preserving) process. The orthogonal cutting model is an initial approximation of the actual process of chip formation in rocks. Motion of the material parallel to the cutting edge is ignored in this model. Shear takes place along a plane that extends from the tool tip to the outer apex of the chip on the free surface. In metals, this assumption is valid only if the chip does not curl to maintain material continuity.

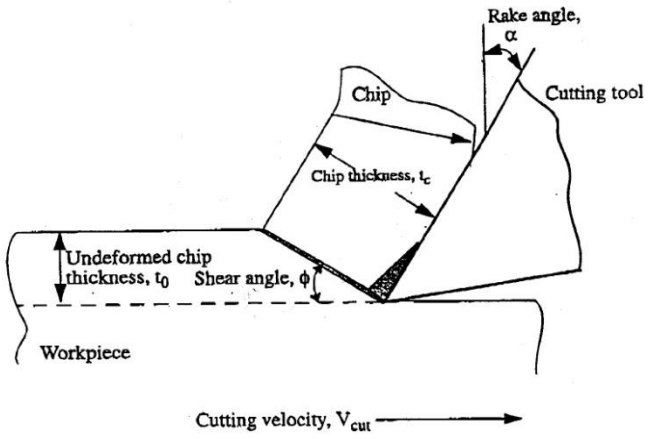

Fig. 2.1: Orthogonal model of cutting in metals [4]

Piispanen's [5] "Deck of cards" model presented a way in which metal is sheared into chips. Later researchers found that it is impossible for the Piispanen model [5] to operate in plane plastic strain at constant plastic volume without the creation of new surface at the tip of the tool. This means there has to be a gap of at least the thickness of the shear band that releases the material to be sheared. Earlier researchers believed that the work required to create a gap could be neglected. Atkins [5] suggested that during steady deformation when surface work is significant, total work will be formed by plasticity along the shear plane, friction along the underside of the chip at the tool interface, and formation of a new cut surface. This study theoretically proved that the primary shear plane angle depends on the material as well as the tool rake angle and friction.

Astakhov et al. [6] in their studies of metal cutting concluded that reduction in plastic deformation during the cutting process increases the efficiency of the process. Also, the final shear strain is not a relevant characteristic to assess plastic deformation in metal cutting since it does not correlate with the known properties of the material.

Xue et al. [7] described three types of failure modes observed in granular materials: flow type, shear type, and tear type. These failure modes occur simultaneously during the cutting process due to the complex nature of rock materials. As the cutting force increases, the rock in front of the cutter is compacted and makes a core. Forces are transmitted to the rock by discrete point load, which finally results in the formation of a micro-crack and tensile crack.

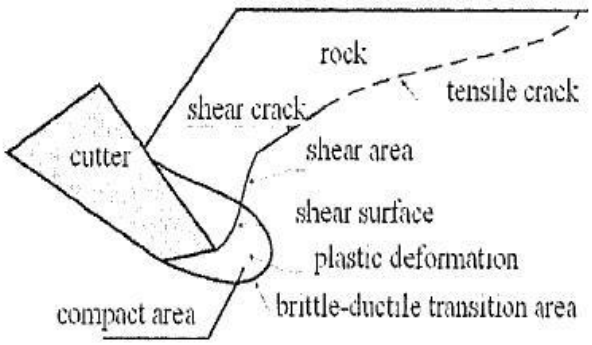

Fig. 2.2: Diagram of rock failure [7]

On the basis of Evans [8] wedge cutter model, Xue et al. [7] studied the cutting of soft rocks including the effect of the formation of a rock compacted core in front of the cutter and friction between the cutter and

the rock (See **Fig. 2.2**). Assuming that rock fragmentation was due to tensile stress and that the resultant force of tensile stress in the fractured surface passes through the center of the arc of failure, Xue et al. obtained expressions for horizontal cutting forces and the vertical propulsive force the for shield cutter.

Romero [9] explained that brittle failure of rocks is due to the concentration of tensile stresses at the edges of the micro-structures found at the points of contact of the crystals. When the applied or resultant stresses in the samples are equal to the maximum that can be resisted by the internal bonds in the crystal, a failure occurs. This failure depends on many factors including grain size, type of internal bonds, size of pre-existing cracks, and density of rock mass.

He also concluded that any type of rock behaves as an entirely cohesive material with a small friction angle at very high pressure (of the order of thousands of atmosphere).

Gray et al. [10] in their laboratory experiments also incorporated a high speed Polaroid camera to capture the actual real time rock cutting process of dry limestone. The initial orientation of the cracks responsible for generating a chip depends on the externally applied loads on the cutter. Normally, the initial fracture orientation is downward, extending below the plane of cutting. Looking at the linear and angular motion of

the chips, they suggested that the failure mode is of tensile nature. It was concluded that for positive rake angles small increase in vertical loading results in a large depth of cut and cutting speed has no appreciable effect on maximum forces.

Zeuch et al. [11] concluded from laboratory experiments that the mechanism of chip formation shown by chip morphology, fracture surface, and sub-surface damage are the same for very different kinds of rocks. The initiation of the fracture responsible for chip formation must occur in advance of the compressed zone. They argued that the superposition of the shearing forces on a rigid indentor compresses the material in advance of the leading edge of the indentor and tends to put it in tension at the trailing edge.

Wei et al. [12] studied the cutting process of diabase and granite (see **Fig. 2.3**). They mentioned the following stages involved in the process of rock fracture under indentation: building up of the stress field, formation of an inelastic deformation zone or a crushed zone, chipping and crater formation at the surface, and formation of subsurface cracks. It was concluded that the diabase cutting process is different from that of granite due to different properties and mineral structures of the rocks. In both rocks crushed zone, cracks, and chipping form under the action of

tensile stress, but the main crack in diabase may develop under the mixed action of tensile stress and shear stress.

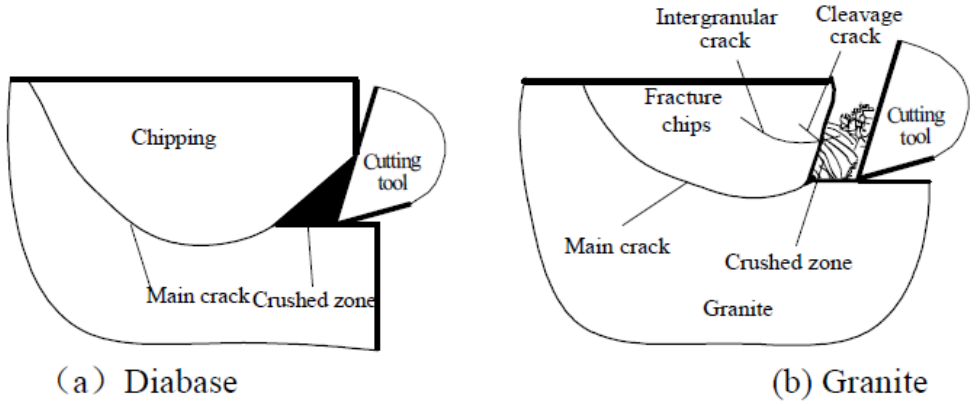

Fig. 2.3: Models of rock cutting mechanism for (a) diabase and (b) granite [12]

Guo et al. [13] concluded that major chip formation in rocks is the result of progressive crack propagation which starts in the vicinity of the cutting tip. Cracks follow a curved path instead of a straight path. The curved path is initially inclined downward and slowly approaches the horizontal free surface of the rock. Cracks tend to propagate deeper if the rake angle is larger. In addition, as the rake angle increases, the tensile stress concentration at the crack tip also increases, which indicates that with the increase in rake angle the requirement of cutting forces decreases. It was also concluded that a large rake angle could assist in generating efficient unstable crack propagation while a small rake angle favors stable crack propagation. Unstable cracks are those cracks that continue to propagate beyond the lowest point in their path without further increase in load, and stable cracks are defined as cracks that

require an increase in load to maintain their propagation in any position of the crack propagation path. Fracture mechanics provides a good insight into the cutting process including detailed information on rock progressive failure and the conditions under which it occurs. This includes the crack propagation path, corresponding load requirements, and stability of the crack propagation.

Yotaro and Kenji [14] identified failure mechanisms in soil cutting and distinguished them as the shear type, the flow type, and the tear type (see **Fig. 2.4**). A fourth mechanism can also be included as the curling type which is common in metal cutting[15]. The flow, tear, and curling types of failure mechanisms are frequent in clay, whereas rocks exhibit tear type, flow type, and shear type failure. Flow type failure occurs when the rocks are under high hydrostatic pressure. Shear type failure occurs when rocks have a low angle of internal friction. Shear type failure is not a continuous process but the shear planes occur so frequently that it is considered as a continuous process.

Miedema [15], to derive the expressions of cutting forces, assumed that the stress on the shear plane and the cutter are constant and uniformly distributed. It was also stated that during the cutting process of sands, the pore volume increases, which is caused by the dilatancy phenomenon.

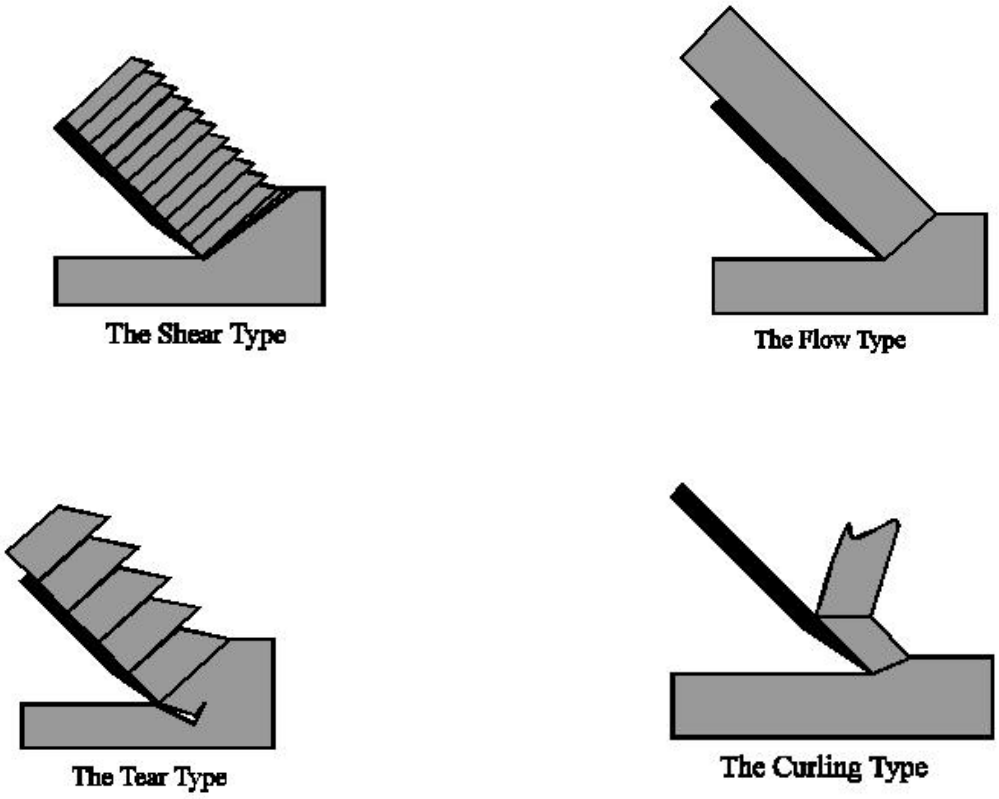

Fig. 2.4: Failure mechanism [14]

Oxley et al. [16] illustrated the formation of a continuous chip by plastic deformation in ductile materials. Two deformation zones, primary and secondary, were defined. Deformation starts when material enters the primary zone from the lower boundary (CD in **Fig. 2.5**) and this deformation continues until it passes the upper boundary (EF in Fig. 2.5). It is known that primary plastic deformation is limited in a finite sized shear zone. Oxley et al. [16] assumed that the primary zone is a parallel sided shear zone. A secondary deformation zone is adjacent to the tool-chip interface that is caused by high contact pressure and frictional force. Material is also deformed in the secondary deformation

zone after exiting the primary deformation zone. Oxley [16] assumed that the secondary deformation zone is a constant thickness shear zone, but in later studies Ozel et al. [17] assumed this zone to be a triangularly shaped zone in which the maximum thickness is proportional to the chip thickness.

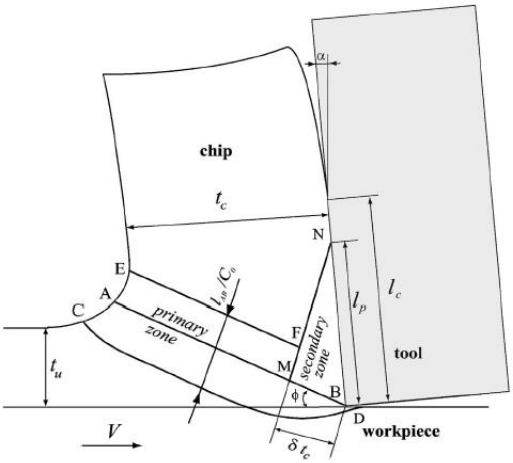

Fig. 2.5: Deformation zones in orthogonal cutting [16]

Nishimatsu [18] proposed that the mode of failure in rock cutting is brittle. From the past work on rock cutting mechanics he assumed that cutting speed has no effect on the mechanics of rock cutting.

As the tool is pushed hard into the rock mass (see **Fig. 2.6**), a crushed zone is generated near the tool edge. This crushed zone is pushed against the rake face of the cutting tool as the tool edge is pressed harder into the rock mass. During this process, the crushed zone is re-compacted and sticks to the tool. This zone is termed as the primary

crushed zone. In metal cutting this primary crushed zone acts like a "built-up edge". As the penetration of the tool edge increases, cutting forces also increase. At a critical value of depth of penetration, a state of stress is generated that allows the propagation of a macroscopic failure crack. Initiation and propagation of this crack results in the formation of a coarse cutting chip.

As the coarse chip forms and the tool moves forward, a peak remaining in the lower part of the initiation point of the macroscopic failure crack is crushed to a fine cutting chip. This is termed as the secondary crushed zone.

After the formation of the secondary crushed zone, without any significant resistance the tool goes on into the overcutting zone until the tool edge is forced against the next rock mass formed by the macroscopic failure crack. This starts a new cycle of the rock cutting process.

During a cycle of rock cutting, as the depth of penetration increases, cutting force also increases to a maximum at the initiation of the macroscopic failure crack, and cutting force decreases suddenly when this maximum has been reached. The formation of the secondary crushed zone is explained by the fact that the macroscopic failure crack starts from a point near the upper limit of the primary crushed zone and does not start from the lowest point of this zone.

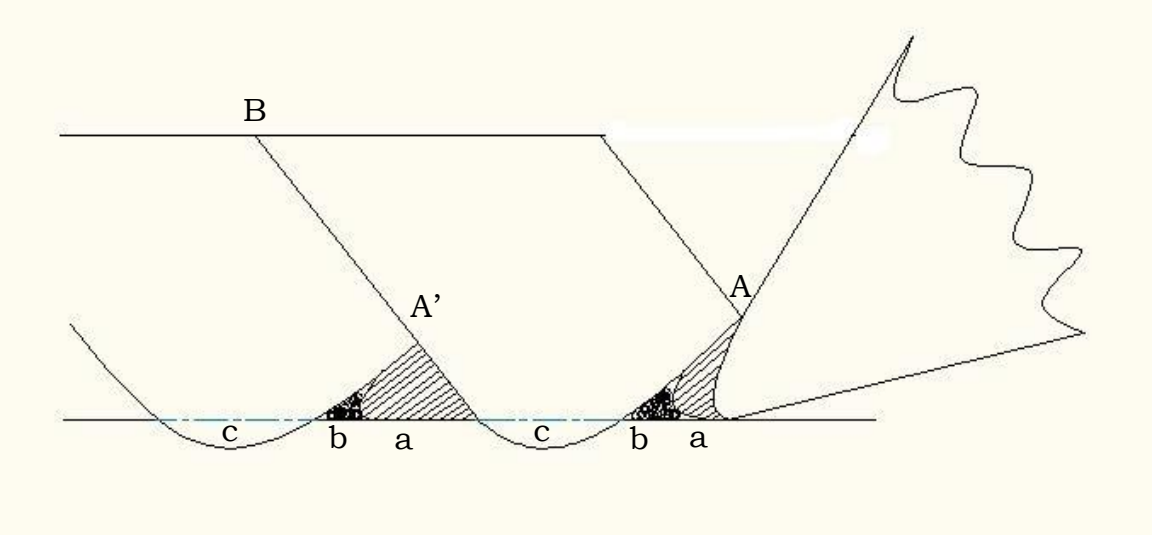

Fig. 2.6: Failure process of rock cutting [18]

Jonak et al. [19] presented the schematic of brittle material cutting deformation of a metal plate during penetration of a cutting tool **(Fig. 2.7).** They also distinguished zones of compression and tension together with the convex zone (boundary/line 2 on Fig. 2.7).

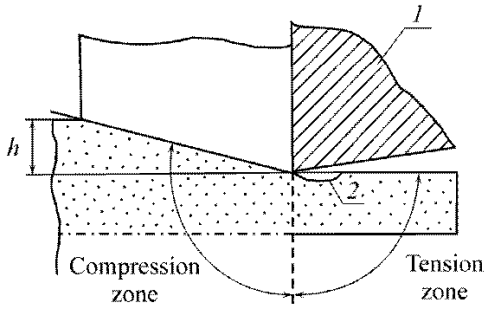

Fig. 2.7: Schematic of metal plate deformation [19]

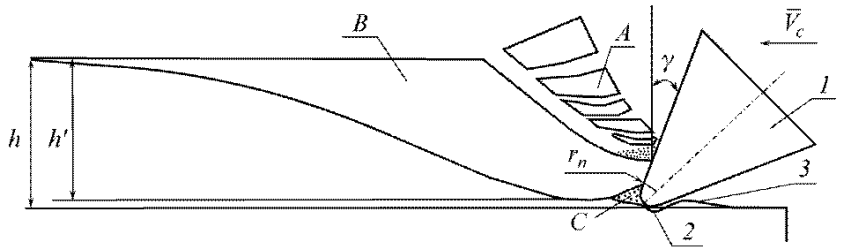

Fig. 2.8: Chip formation in cutting natural brittle materials [19]

Fig. 2.8 shows experimental results from a study for brittle material cutting. A sharper tool was used to penetrate the rock. 'A' represents the fine chip element zone; 'B' is the main chip element formation zone; 'C' is the crushed material zone. The convex down arc of the boundary and the convex up arc of the boundary is shown by 2 and 3, respectively. As the load on the penetrating wedge increases, discontinuity of the surface takes place and premature failure occurs. A transition layer consisting of fine crushed particles of the material is formed in the vicinity of the cutting edge of the tool. Due to the high porosity of rocks, this layer changes the nature of interaction between the tool and the material. Simulation using a nonlinear (elasoplastic) model gives results similar to metal cutting.

Lei et al. [20] developed a methodology to apply hydrostatic pressure to the rock sample during the orthogonal cutting simulation using DEM. Simulation results showed that plastic deformation is promoted after applying the hydrostatic pressure.

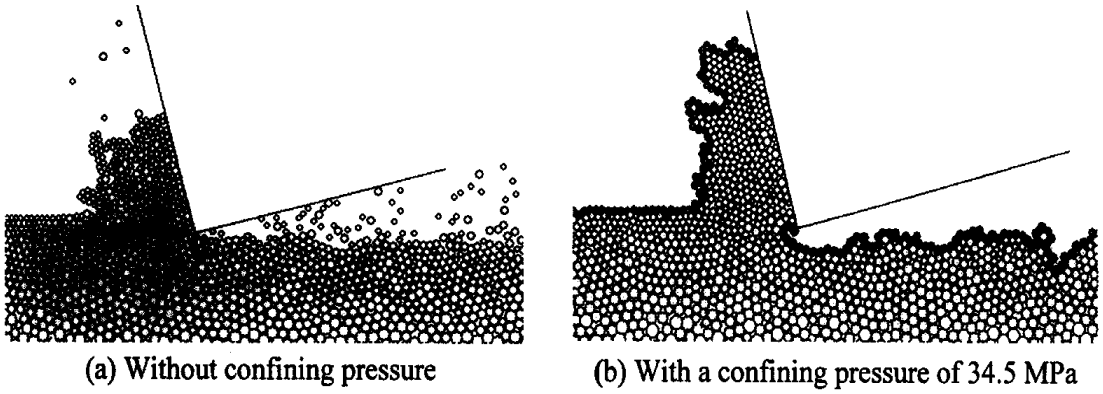

Fig. 2.9: Chip formation (a) without confining pressure and (b) with confining pressure [20]

Lei et al. [20] showed with their simulations that when a confining pressure was applied to the rock mass during cutting (confining pressure was 34.5 MPa), a dense chip and machined surface formed (see **Fig. 2.9**). It was observed that no large cracks were visible in the chip and beneath the machined surface. This was in contrast to what was seen without application of the confining pressure. It can be seen from the Fig. 2.9 that without confining pressure many balls had broken loose and flown away from the rock mass. Large fractures were present with short chip formation in the front of the cutting edge of the tool.

Lei et al. [20] also showed that cutting forces fluctuate in both the cases of unconfined and confined simulations. Cutting with a confining pressure indicated a larger force magnitude to overcome the hydrostatic pressure and suppressed crack propagation. Average force increase with

the magnitude of the negative rake angle was attributed to the increased degree of difficulty in chip flow for a large negative rake angle.

Menezes et al. [21] used a commercially available FEM code, LS-DYNA to simulate discontinuous chip formation in rock cutting. It was shown that the tool initially indents the rock. During the cutting process, chips started to form and finally they separated from the rock mass. The size and morphology of the chips changed with the depth of cut. The size of the discontinuous chips increased with increasing depth of cut. It was shown that initiation of the fractures occurs from the tool edge and then fractures extend ahead of the tool. As the fractures extend closer to the rock surface, it results in the formation of a chip. It was also stated that, due to a mismatch in elastic properties between the cutter and the rock, at the beginning of the loading, a highly confined and pressurized zone forms near the cutting tool tip. Fractures develop quickly in the upper area of the rock rather than into the rock along the horizontal direction. As fractures develop and the chip starts to form, the highly stressed zone ahead of the cutter becomes less confined and less stressed. A complicated stress state is responsible for the chip formation as elements fail in shear and tension mode. Morphology of the chips is dependent on the characteristics of the rock mass, tool geometry, and cutting parameters.

Shenghua [22] developed a two dimensional simulation model of rock cutting by the finite element method using ANSYS software in which friction between the crack faces and the tool with rocks has been taken into account. From the model, the influence of the friction and multi-cracks on the cutting force can be determined. The model proved the empirical model of Evans and the analytical method of Nishimatsu.

Block et al. [23] established that chip morphology and the mode of failure changes at high confining pressures. At low confining pressure brittle failure is responsible for the chip formation while at high confining pressure ductile failure is accountable for the chip formation. It was concluded that the lost energy increases rapidly as the depth of cut increases in the process of ductile failure.

Brett et al. [24] in their analysis of bit wear emphasized that only a certain maximum weight on bit can be supported by the cutter without damage to the cutter. If the bit is in the process of cutting a soft rock, loads on the cutter face are distributed across the cutter face; if cutting a hard rock, loads on the cutter are concentrated such that only the lip of the cutter is taking the entire load (see **Fig. 2.10**). It is shown that stress is two to three times higher in the harder rocks.

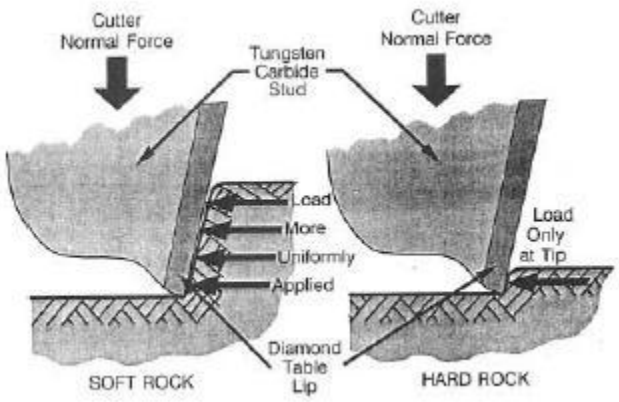

Fig. 2.10: Lip schematic in soft and hard formation [24]

In the literature, most of the researchers agree that indentation of the cutting tool causes crushing of the rock and a compressed zone is formed. At the same time most of them neglect this compression of rock in their analysis. There are arguments on what causes the failure of rock. Olson [4], Atkins [5], Miedema [15], Oxley [16], and Nishimatsu [18] believe that the failure happens due to shear stress while Gray et al. [10] and Romero [9] did their analysis on the basis of failure caused by tensile failure. Also, it is common to believe that the rock cutting process is complex in nature and brittle failure of the rock is caused by a mix of shear and tensile stresses at different stages in the cutting process. Zeuch et al. [11], Wei et al. [12], and Menezes [21] supported this hypothesis. These differences show that rock cutting process is yet to be understood in full.

As the cutting process is yet to be fully understood, and bit designs are approved on the basis of lab experiments and field-testing, it would convenient to have a parameter that collectively takes care of the drilling process with particular bit design. The purpose is to fully utilize a running bit even if we don't know the actual conditions in the bottomhole. Mechanical specific energy has been seen to help drilling engineers evaluate the condition of a bit and take an appropriate action. In this work focus is on understanding the dependence of mechanical specific energy on the bottomhole pressure conditions.

2.2 Models of Rock Cutting

Merchant [25] presented the first model of cutting for the metals. Later on researchers modified this model for the application in rock cutting. Evans [8] introduced a model on the basis of his observations on the coal cutting. Nishimatsu [18] presented a model for rock cutting assuming that stress would be severe near the tool cutting edge and resultant stress would decrease from the cutting edge of the tool to the surface along a line. Different models of cutting are briefly described below:

2.2.1 Merchant Model

Merchant [25-26] developed a model to calculate the cutting force in the metals. He was the first to introduce a model for metal cutting. Many researchers later used Merchant's theory to develop more sophisticated models.

The Merchant model is semi-empirical in nature. In his theory, it is assumed that failure is caused by shear stresses in orthogonal cutting where cutting edge of the tool is perpendicular to the direction of its motion. The cutting tool generates a finished surface that is parallel to the original surface of the material being cut. Shear takes place in a plane which starts from the tip of the cutter to the surface of the metal making an angle θ from the horizontal. When compared to the width of

the cutting tool, depth of cut is very small, and hence a condition of plane strain is assumed. This original Merchant theory has been extended to the rock cutting. Experiments show that Merchant's model can be used to describe the cutting processes of some coals and wet chalk.

Fig. 2.11 shows the forces acting on a chip generated in the orthogonal cutting process. Merchant assumed that the chip is in equilibrium due to force acting on it.

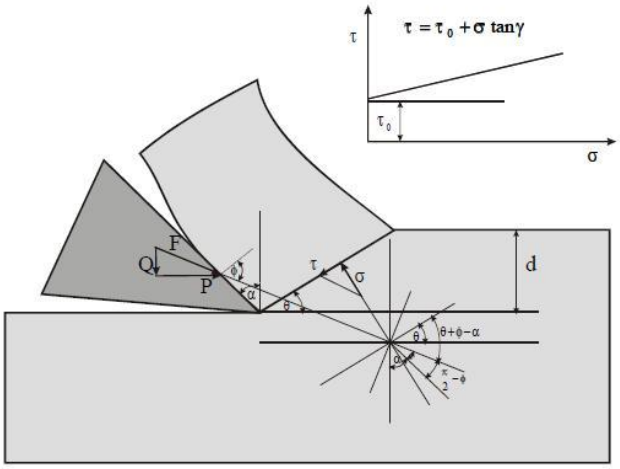

Fig. 2.11: Merchant model of cutting [26]

Force equilibrium on the chip gives

$$\sigma = \frac{\sin\theta}{d} F \sin(\theta + \phi - \alpha)$$

Also,

$$\tau = \frac{\sin\theta}{d} F \cos(\theta + \phi - \alpha)$$

where

σ is shear stress;

τ is normal stress;

θ is angle made by failure plane with horizontal;

d is depth of cut;

F is resultant force from the wedge acting on the chip;

ϕ is angle of resultant force with the normal; and

α is rake angle.

At failure,

$$\tau = \tau_0 + \sigma \tan\gamma$$

where τ_0 is cohesion and γ is the angle of internal friction of the rock.

Using the values of σ and τ in the failure equation gives,

$$F = \frac{\tau_0 \, d \cos\gamma}{\sin\theta \cos(\theta + \phi - \alpha + \gamma)}$$

Then, for a given angle θ, force F should be minimized with respect to θ:

$$\frac{dF}{d\theta} = \frac{d}{d\theta}\left(\frac{\tau_0 \, d \cos\gamma}{\sin\theta \cos(\theta + \phi - \alpha + \gamma)}\right)$$

which gives,

$$\theta = \frac{\pi}{4} - \left(\frac{\phi - \alpha + \gamma}{2}\right)$$

using the value of θ in the expression of resultant force F,

$$F = \frac{2\,\tau_0 d\cos\gamma}{1-\sin(\phi-\alpha+\gamma)}$$

and cutting force (F_c) as,

$$F_c = \frac{2\,\tau_0 d\cos\gamma\cos(\phi-\alpha)}{1-\sin(\phi-\alpha+\gamma)}$$

2.2.2 Evans Model

Past research shows no physical similarity between coal breakage and metal cutting [8, 26]. Chip formation is an integral and important part of metal cutting process; this process cannot be seen during coal cutting experiments. Evans, based on the observations made during coal cutting with penetrating wedges, acknowledged that mode of wedge entry in the coal is by crushing only. Evans also argued that cracks originate from the tip of wedge due to tensile breakage.

Evans considered a wedge of angle 2θ as shown in **Fig. 2.12**. He observed that coal breakage was along the curve CD. He assumed curve CD as a circular arc of radius r; and that the curve has a horizontal tangent at C since it was observed in the experiments that most prominent cracks are generated along the direction of the resultant load. Evans presumed a force passing through point D to keep the coal block in equilibrium as seen in the Fig. 2.12.

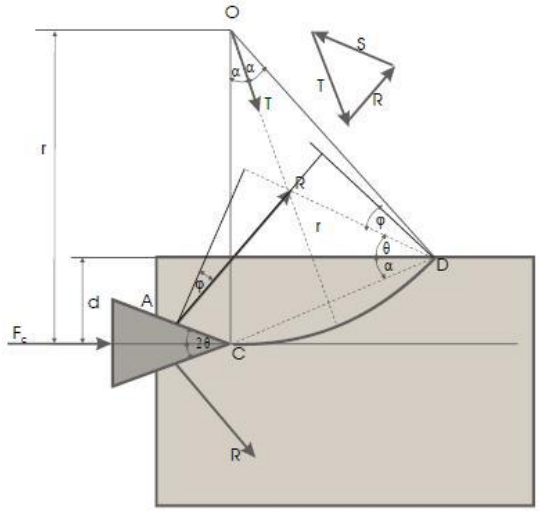

Fig. 2.12: Evans model of cutting [26]

Here, Evans assumed that a state of plain stress prevails in the deformation process. Considering the equilibrium of a slice of coal of unit thickness, the force due to tensile strength of the rock is given by,

$$T = \int \sigma_t \cos\omega \; dr$$

and

$$T = \int_{-\alpha}^{\alpha} \sigma_t \, r \cos\omega \; d\omega = 2 \, \sigma_t \, r \sin\alpha$$

where

$rd\omega$ is an element on the arc CD;

ω is an angle that arc CD makes with radius of symmetry (see Fig. 2.12);

σ_t is tensile strength of the rock; and

α is half angle of arc CD.

Taking moment about point D,

$$R \frac{d}{\sin \alpha} \cos(\alpha + \theta + \varphi) = Tr \sin \alpha$$

where

R is the force acting on the surface of wedge;

d is depth of cut; and

φ is the angle force R makes with the normal to the surface of wedge.

Also,

$$2\, r \sin \alpha = \frac{d}{\sin \alpha}$$

This gives

$$R = \frac{\sigma_t\, d}{2 \sin \alpha \cos(\alpha + \theta + \varphi)}$$

which gives cutting force as:

$$F_c = \frac{\sigma_t\, d \sin(\theta + \varphi)}{\sin \alpha \cos(\alpha + \theta + \varphi)}$$

2.2.3 Nishimatsu Model

Nishimatsu [18] stated that no plastic deformation occurs during rock cutting, and that the mode of failure taking place in rock cutting is brittle. He also noted that cutting speed has no effect on the mechanics of rock cutting. Also, due to the brittle nature of rock, he assumed that the state of stress in the rock mass will not be uniform.

Nishimatsu [18] also assumed that the mechanics of rock cutting can be treated as a two-dimensional problem since width of the cutting edge is much greater than the depth of cut. Such an assumption satisfied the conditions of orthogonal cutting.

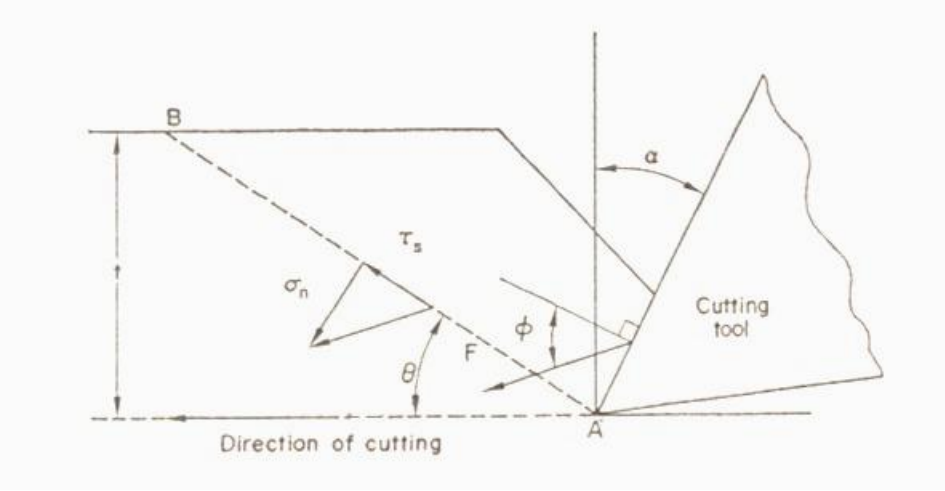

Fig. 2.13: The stress and cutting forces for rock cutting [18]

Fig. 2.13 shows the shear plane as AB. Stress concentration would be most severe near the tool cutting edge, and the resultant stress would decrease from the cutting edge of tool to the surface along the line AB.

Nishimatsu assumed that the magnitude of the resultant stress acting on the unit length of the line AB is given by

$$P = P_o \left(\frac{t}{\sin\theta} - \lambda\right)^n$$

where

P_o is a constant determined from the equilibrium of state;

t is depth of cut;

θ is the angle between the direction of cutting and the line AB;

λ is the distance from the edge point A to an arbitrary point on the line AB; and

n is the stress distribution factor (i.e. a constant concerned with the state of stress in the rock-cutting process).

Also, Nishimatsu assumed that the direction of the resultant stress P is constant along the line AB, and the integration of this resultant stress P along the line AB should be in equilibrium with the resultant cutting force.

Thus,

$$F + P_o \int_0^{\frac{t}{\sin\theta}} \left(\frac{t}{\sin\theta} - \lambda\right)^n d\lambda = 0$$

where F is the resultant cutting force. Integrating the second term in the above equation, yields

$$F + P_o \frac{1}{n+1} \left(\frac{t}{\sin\theta}\right)^{n+1} = 0$$

which gives

$$P_o = -F\,(n+1)\left(\frac{t}{\sin\theta}\right)^{-(n+1)}$$

and

$$P = -(n+1)\left(\frac{t}{\sin\theta}\right)^{-(n+1)} F\left(\frac{t}{\sin\theta} - \lambda\right)^{n}$$

Taking the normal and tangential components of the resultant stress P,

$$\sigma_{n0} = -(n+1)\left(\frac{t}{\sin\theta}\right)^{-(n+1)} F\left(\frac{t}{\sin\theta} - \lambda\right)^{n} \sin(\theta - \alpha + \phi)$$

where α is the rake angle of the cutting tool and ϕ is the angle between the direction of the resultant cutting force and the normal to the rake face of the cutting tool termed as “the angle of friction of rock cutting”.

For $\lambda = 0$, the maximum normal stress is

$$\sigma_{n0} = -(n+1)\left(\frac{t}{\sin\theta}\right)^{-1} F \sin(\theta - \alpha + \phi)$$

Similarly, maximum shear stress at $\lambda = 0$ is given by

$$\tau_{s0} = -(n+1)\left(\frac{t}{\sin\theta}\right)^{-1} F \cos(\theta - \alpha + \phi)$$

Nishimatsu [18] assumed that the brittle rocks follow Mohr's criterion of failure, given by

$$\pm \tau_s = S_s - \sigma_n \tan k$$

where S_s is shear strength and k is a constant of the angle of internal friction. In this study, Nishimatsu has taken compressive strength negative. Assuming that the normal stress acting on the line AB is compressive and considering the fact that cutting forces should be positive, it is clear that $\theta > \alpha - \phi$, which gives $\tau_s < 0$ and hence the negative sign should be adopted on the left hand side of the above equation. Thus, above equation takes the form

$$-\tau_s = S_s - \sigma_n \tan k$$

Using the values of τ_s and σ_n, Nishimatsu [18] obtained

$$(n+1)\frac{\sin\theta}{t} F \cos(\theta - \alpha + \phi) = S_s + \tan k \ (n+1)\frac{\sin\theta}{t} F \sin(\theta - \alpha + \phi)$$

$$F = -\frac{1}{n+1}\left(\frac{t}{\sin\theta}\right)\left[\frac{S_s}{\tan k \sin(\theta - \alpha + \phi) - \cos(\theta - \alpha + \phi)}\right]$$

Assuming that the direction of the line AB on which the failure stress acts should minimize the cutting force (or the work done while cutting). Differentiating the above equation with respect to θ

$$\frac{dF}{d\theta} = 0$$

gives

$$2\theta = \frac{\pi}{2} - (k - \alpha + \phi)$$

Now, we can replace θ in the following equation,

$$F = -\frac{1}{n+1}\left(\frac{t}{\sin\theta}\right)\left[\frac{S_s}{\tan k \sin(\theta - \alpha + \phi) - \cos(\theta - \alpha + \phi)}\right]$$

giving us resultant cutting force F

$$F = \frac{2}{n+1} S_s\, t\, \frac{\cos k}{1 - \sin(k - \alpha + \phi)}$$

and yields cutting force F_c as,

$$F_c = \frac{2}{n+1} S_s\, t\, \frac{\cos k}{1 - \sin(k - \alpha + \phi)} \cos(\phi - \alpha)$$

2.3 Discussion on Single Shear Plane Models

Researchers commonly mentioned that single shear plane models are ideal. However, there is no account available in the literature on how far it deviates from the real processes. Briks, as cited by Astakhov [27], provided reasons why a single shear plane cannot exist: he argued that due to instant chip formation, an infinite high stress gradient must be present. Also, since, the velocity of the particles of the layer being removed changes; this layer should be subjected to infinite deceleration. He suggested that these concerns might be resolved by assuming a deformation zone, which consists of a family of shear planes.

Because it involves shearing, Zorev [27-28] considered the deformation process being characterized by the lines of maximum shear stress. He concluded that it is very difficult to determine the stressed and deformed state in the deformation zone because there is no steady state mode of deformation due to the ever-changing shape of the deformation zone.

Astakhov [27] argued that the velocity diagram associated with Merchant's model is faulty, and corrections in the velocity diagram (by changing the velocity signs) resulted in the generation of energy instead of consumption of energy during the cutting process. Astakhov [27] argued that velocity diagram has the velocity components from different coordinate systems.

Similarly, the limiting frictional coefficient cannot be verified with experimental data and simulation results. Surprisingly, most simulations achieve good matching with the experimental results despite using particular value of friction that is below the limiting value for the sliding friction.

It is also important to note that in his convenient force diagram, Merchant [25] shifted the resultant force parallel to itself, which resulted in loss of moment equal to force time shift distance. Astakhov [27] proved that this missing moment is the main cause for chip formation and showed it experimentally and theoretically. He opined that this missing moment is also directly involved in the chip curling process and can be helpful in explaining the chip curling process.

Moreover, results obtained from the single shear plane models deviate significantly from the experimental results, which was highlighted in Pugh's [29] experiments.

CHAPTER III

ROCK DRILLABILITY

3.1 Rock Mechanical Properties

The most used properties of the rocks are unconfined compressive strength and confined compressive strength. A brief description is given below:

3.1.1 Unconfined Compressive Strength

The test to obtain the unconfined or uniaxial compressive strength [30-31] has been the most sought quantitative method to characterize rock strength. Even at present this test is the basis of many rock classifications, but in the case of field characterization it has been replaced by the simpler point-load method. ASTM designation D2938 recommends the specifications for the test apparatus, instrumentation, and the steps involved to carry out the unconfined compressive strength test.

Fig. 3.1: Common laboratory schematic for unconfined compression test [30]

To carry out this test, a specimen is prepared in the form of a cylinder having a length of two to three times its diameter. Ends of this sample are flat, smooth, and perpendicular to the cylinder axis. These samples are usually prepared by cutting cores from a large piece of rock. After the samples are ready, they are compressed between the crosshead and platen of the testing machine in which the platen is used to apply the load. The load is increased steadily and the rock samples fails when the applied load equals to the unconfined compressive strength of the rock.

If the peak load is P and the initial cross-sectional area of the sample is A, the compressive strength of the rock (q_u) is defined as the ratio of peak load to the initial rock sample cross-sectional area.

$$q_u = \frac{P}{A}$$

3.1.2 Confined Compressive Strength

Confined compressive strength [30] of the rock material is derived from a confined compression test or triaxial compression test. In this test, a cylindrical sample is loaded vertically, simultaneously with an axisymmetric confining pressure. Test procedures to carry out a triaxial compression test are recommended by ASTM designation D2664-67.

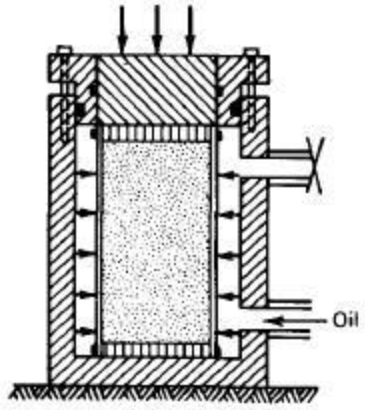

Fig. 3.2: Common laboratory schematic for triaxial compression test [30]

If P is the peak load, A is the initial cross-sectional area of the rock sample and p is the confining pressure, stress conditions are defined as

$$\sigma_1 = \frac{P}{A}$$

$$\sigma_2 = \sigma_3 = p$$

In a triaxial test, a rock sample is subjected to a confining pressure which is achieved by enclosing the sample in an impervious jacket and applying a uniform confining pressure with a hydraulic fluid. Hydraulic

fluid ensures the equal confining pressure on the rock sample from all directions. In these conditions intermediate stress (σ_2) and minimum stress (σ_3) are equal to each other and confining pressure (p). Due to confining pressure, the rocks show a strengthening effect.

Usually to conduct a triaxial compression test, confining pressure (p) is applied to the jacket which infers that $\sigma_1 = \sigma_2 = \sigma_3 = p$ and then an axial load of, $\sigma_1 - p$ is applied keeping the horizontal pressure (p) constant.

3.2 Failure Criterion in Rocks

3.2.1 Mohr Coulomb Failure Criterion

As the confining pressure to the rock increases, the strength of the rock also increases and in a similar way peak stress of the rock increases for the same reason. On this basis a criterion of failure can be characterized by taking into account the variation of peak stress (σ_1) with the confining pressure (σ_3). Mohr-Coulomb criterion [30] is the simplest and most commonly used criterion of failure.

Mohr suggested that the normal stress (σ) and the shear stress (τ) across a plane, where shear failure takes place, are related by a relationship that is characteristic of rock material. This relationship can be represented by a curve which is tangent to all the Mohr's circles representing critical combinations of principal stress at the time of

failure. We know that Mohr's circles are defined by the peak normal stress and confining pressure.

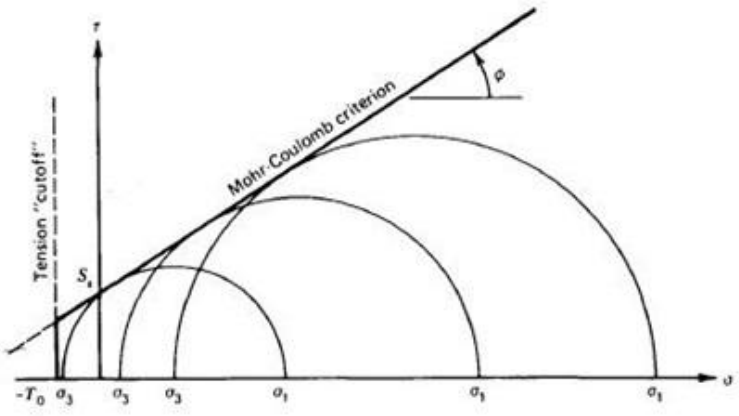

Fig. 3.3: The Mohr-Coulomb failure criterion [30]

The failure envelope of the material can be expressed as an equation of a straight line in terms of normal and shear stresses on the plane represented by the point of tangency of a Mohr circle with the envelope.

$$\tau_p = \sigma \tan \phi + S_i$$

This equation gives a relationship between peak shear stress (τ_p) or shear strength and normal stress (σ). The slope of the line is a function of angle of internal friction (ϕ), which is a characteristic of the material. The y – intercept of the equation S_i, is termed as residual shear stress or cohesion.

Failure of the rock takes place when applied normal and shear stress lie above or on the Mohr-Coulomb failure envelope. The rock will not fail if

applied normal and shear stress lie below the Mohr-Coulomb failure envelope.

3.2.2 Griffith Theory

Griffith [32-33] suggested that in brittle materials, there are microscopic defects present in the form of small cracks, fissures, and grain boundaries. These natural flaws are termed as "Griffith" cracks. When stress generated at the ends of theses microscopic defects exceeds tensile strength of the material, fractures initiate from the ends. Griffith theory predicts a parabolic failure envelope.

Griffith applied this theory to a plate of uniform thickness, having an elliptical flaw at right angles to the direction of loading, which was subjected to a uniaxial tensile stress. He later extended his theory to a plate subjected to compressive stresses σ_1 and σ_2.

Griffith's Criterion gives:

$$(\sigma_1 - \sigma_3)^2 = 8\,T\,(\sigma_1 + \sigma_3) \qquad \text{if } \sigma_1 + 3\,\sigma_3 \geq 0$$

$$T = \sigma_3 \qquad \text{if } \sigma_1 + 3\,\sigma_3 < 0$$

Griffith theory gives a parabolic failure envelope which is observed by the intact rocks. Even if Griffith theory gives a failure envelope of the general form, due to the reason of not considering the friction forces in the

natural defects, the theory does not provide a model which appeals to researchers. Even modifying the Griffith theory by including the friction forces on closed defects have not given results to match with experimental observations.

Later on Murrell [34] modified the Griffith criterion for the case when uniaxial compressive strength is 8 times the uniaxial tensile strength. That gives

$$(\sigma_1 - \sigma_3)^2 - 8T(\sigma_1 + \sigma_3) = 16T^2$$

3.2.3 Empirical Strength Criteria for Intact Rock

Various researchers worked on the strength criterion of the intact rocks. Few of them are presented here.

Hoek–Brown Criterion

Hoek and Brown [35] presented their strength criterion in the form of

$$\sigma_1 = \sigma_3 + \sigma_c \left(m \frac{\sigma_3}{\sigma_1} + 1 \right)^{0.5}$$

where σ_c is unconfined compressive strength of intact rock, σ_1 is major principal stress, σ_3 is minor principal stress, and m is constant for the intact rock in consideration, which depends on the rock texture and mineralogy. In general, m depends on the degree of interlocking between

blocks in the jointed rock mass and has a range from 27.9 for granite to 5.4 for limestone.

Yudhbir Criterion

Yudhbir et al. [36] found that in the brittle range Hoek and Brown criterion works satisfactory but is not a good fit for ductile range. They proposed a strength criterion as

$$\frac{\sigma_1}{\sigma_c} = A + B\left(\frac{\sigma_3}{\sigma_c}\right)^a$$

where a is in the range of 0.65 to 0.75 while A and B are the functions of rock type.

Johnston Criterion

Based on experimental data of a wide range of materials (ranging from clays to extremely hard rocks), Johnston [37] proposed the following strength criterion for the intact rock:

$$\frac{\sigma_1}{\sigma_c} = \left(\frac{m}{B}\frac{\sigma_3}{\sigma_c} + 1\right)^B$$

B describes the nonlinearity of the strength envelope and is independent of material type. It varies from 1.0 for normally consolidated clays to 0.5 for rocks with strength of σ_c = 250 MPa and is a function of unconfined

compressive strength. *m* describes the slope of failure envelope at $\sigma_3 = 0$ and is a function of both material type and unconfined compressive strength.

3.3 Factors Affecting Failure of Rock

The rock material which would be found in the *in situ* condition cannot be considered as ideal brittle material upon which all the theory is based upon. On the same account, a wide range of conditions which are likely to be encountered in the field cannot be simulated in the carefully selected laboratory test specimen. Hence the laboratory conditions are not representative of field conditions.

If estimates can be made of the extent of deviation to which the rock behavior is likely to be influenced by the deviations from the ideal conditions, an ideal failure criterion can give practical solutions.

3.3.1 Effect of Water Saturation on the Strength of Rock

Saturated water can reduce the strength of the rock significantly by chemically or physically altering its inherent properties. As the water content increases, the unconfined compressive strength of the intact rocks decreases. It has been shown that saturated specimens have the strength that is almost half of the dry specimens and hence this strength reduction is very important [38].

This relationship between water content and unconfined compressive strength is given by Hawkins & McConnell [39].

$$\sigma_c = a\, e^{-bw} + c$$

where σ_c is unconfined compressive strength, w is water content and $a, b,$ and c are constants.

Also, if the water is present under pressure it will reduce the strength of the rock even more. Experimental observations confirm that the presence of pore pressure reduces the normal stress to effective stress which can be obtained by subtracting pore pressure from normal stress.

3.3.2 Effect of Porosity on Unconfined Compressive Strength of the Rock

Strength of intact rock depends significantly on the porosity of the material. As the porosity of the material increases, the unconfined compressive strength of the intact rock decreases. There are empirical relations available which correlate unconfined compressive strength to porosity of the material.

Rshewski and Novik [38] defined unconfined compressive strength as:

$$\sigma_c = \alpha\,(1 - \beta\, n)^2$$

where σ_c is unconfined compressive strength in MPa, n is porosity in % and α and β are constants which can be obtained from test results. Since the density of a material closely depends on the porosity of the material, it also affects the strength of the intact rock. As the density of the intact rock increases, the unconfined compressive strength of the intact rock also increases.

3.3.3 Effect of Normal Stress Upon the Frictional Behavior of the Rock

A set of Mohr's circles obtained by low pressure triaxial compression test on brittle rocks generally gives a failure envelope which can be expressed by a straight line. The assumption that the coefficient of internal friction obtained from this straight line failure envelope is constant holds true only for low confining pressures (up to approximately one-half the uniaxial compressive strength of the rock [38]). This situation is mostly encountered in civil and mining engineering applications.

At a high confining pressure, as encountered in geology and petroleum applications, the assumption of a constant coefficient of internal friction is not valid. It is also not true in the case of soft rocks such as shales and siltstones, which exhibit non-linear failure envelopes even at low confining pressures.

The coefficient of internal friction, as in a straight line failure envelope, is not a constant, but depends upon the magnitude of the normal compressive stress which is corroborated by the studies carried out by Murrell [40], Hobbs [41], Patton [42] and Byerlee [43]. The reason for this is related with the interlocking of asperities on the shear plane. The interlocking depends upon the close contact of the asperities, which, in turn, depends upon the magnitude of normal stress.

Jonak [44] showed that the trajectories of cracks, the shape and size of the chip being generated depend on the coefficient of the friction between chip element and the tool rake face. He used the finite element method to simulate his experiments. This presented the possibility to control the chip formation process by changing the coefficient of friction. A suitably chosen material can minimize the load on the cutter and the energy required for cutting a fixed chip size.

3.3.4 Effect of Anisotropy on the Strength of a Rock

In theoretical discussions, an ideal brittle rock is supposed to contain a large number of randomly oriented natural flaws of equal size. In practical, it is hardly true for most of the conditions [45].

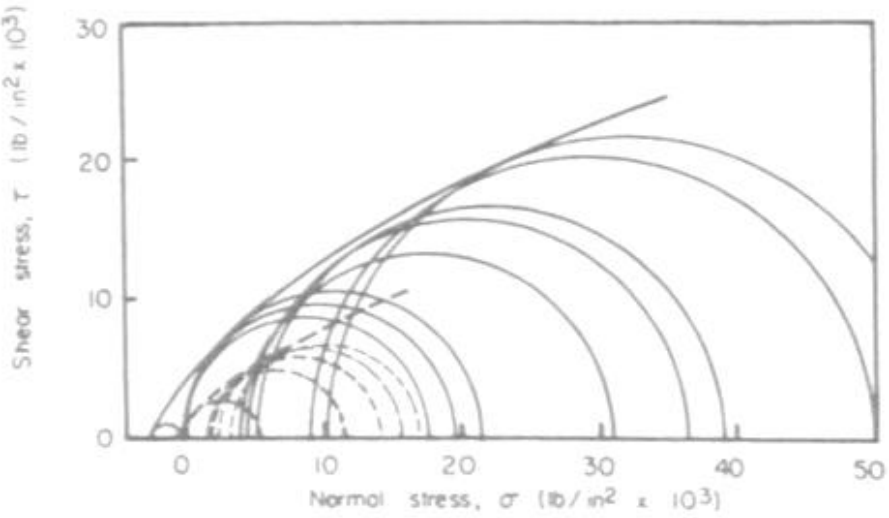

Fig. 3.4: Failure behavior of a South African slate [45]

Fig. 3.4 shows the failure behavior of a South African slate [45]. The solid line represents the tests in which the bedding planes were oriented to minimize their influence, while the dashed line represents the tests in which the bedding planes were oriented to maximize their effect. Fig. 3.4 shows that the failure envelope for the latter case, when slate is in its weakest state, is evidently a scaled down version of the first case when slate is in its strongest state. What this signifies is that depending upon the orientation of the bedding planes, the value of the uniaxial compressive strength of the slate varies by a factor of approximately four. The orientation of the weakening bedding planes is not necessarily known in all cases. In these cases, it can be assumed that the failure envelope will lie in-between two extreme cases of weakest and strongest

orientation state. For all practical purposes, it is suggested to follow the envelope representing the weakest state of rock material.

3.3.5 Effect of Confining Pressure

In most drilling operations, rocks being drilled are subjected to high confining pressures due to heavy drilling mud. Due to this reason, it becomes very important to know how confining pressure will affect the process of rock cutting.

A brittle rock under low confining pressure may become ductile under high confining pressure. Cohesion and internal friction of the rock are responsible for the brittle or ductile behavior [33]. As discussed earlier, internal friction considerably depends on the stress applied, hence the failure behavior of the rock changes at different confining pressures. At low stress conditions, cohesion of the rock plays a significant part in failure, hence rocks are prone to show brittle failure. At high stress conditions, internal friction of the rock takes over and failure behavior changes to a ductile mode. Karman [46] presented his result carried on Carrare Marble (see **Fig. 3.5**) which clearly shows that under 0 MPa confining pressure the rock exhibits a brittle nature. At 85 MPa confining pressure, the rock behaves perfectly as an ideal elastoplastic material, while at very high confining pressures its behavior is strain hardening.

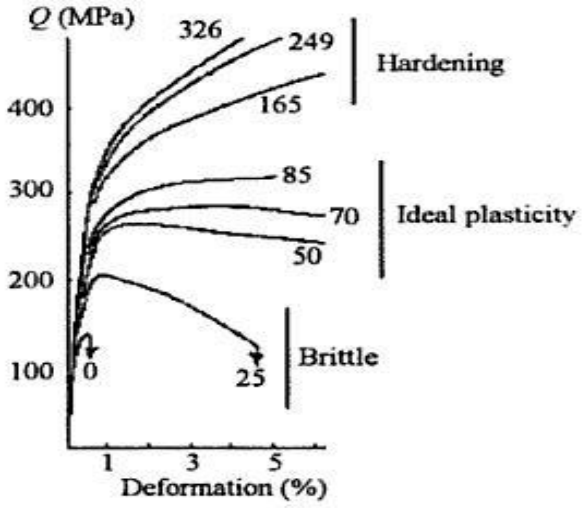

Fig. 3.5: Influence of mean stress on the ductile/brittle transition of Carrare Marble [46]

Lei & Kaitkay [47], used the distinct element method to simulate the cutting of a rock with and without confining pressure. Their results show that with no confining pressure, relatively large cracks/voids exist in the chip and under the machined surface. Small material pieces broke loose and flew away from the bulk material. When confining pressure was applied, there were no cracks/voids found in both the chip and under the machined surface. In contrast, a denser chip and machined surface were generated. Due to confining pressure, in later case, a larger force magnitude was seen in the cutting process. They concluded that confining pressure can effectively restrain crack formation during rock cutting and assists in chip formation.

Kaitkay and Lei [48] showed from their experiments that the increase in confining pressure is accompanied by an increase in chip length and suggested that the cutting process can alter from a dominant brittle fracture to intermediate ductile-brittle fracture. This transformation is responsible to an increase in chip length. Since rocks are constituted of small grains of different shapes and sizes held together at grain boundaries, they proposed that fractures initiate within grains and at grain boundaries due to failure in tension in case when there is no confining pressure is being exerted. The broken grain particles are removed in the form of powder and the chip length is not appreciable. As the confining pressure is applied, failure in shear mode happens and longer chips are assumed to be formed of small rock particles with internal fractures restrained by the applied confining pressure.

3.3.6 Effect of Temperature

Geomaterials change their behavior when exposed to different temperatures. Generally at low temperatures, they exhibit brittle nature while at high temperatures materials behave in a more ductile manner [46] (see **Fig. 3.6**).

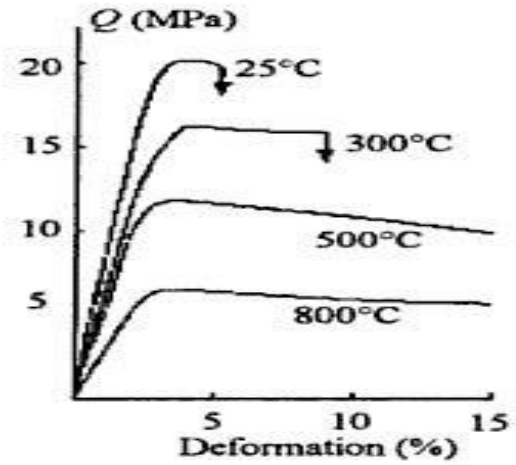

Fig. 3.6: Influence of temperature on the behavior of granite [46]

Fig. 3.6 shows that granite fails in brittle manner at low temperature while its failure mode changes to ductile at high temperature.

3.4 Effect of Bottomhole Pressure Conditions on Drilling

The pressure in downhole conditions plays a big role in the drilling process. A lot of work has been done to understand its effect on different drilling parameters to reduce the risks involved in the drilling process. A further study of the effect of different pressure conditions in the borehole on the mechanical specific energy is still required.

Murray and Cunningham [49] observed an increase in confining pressure results in a decrease in rate of penetration. After a maximum confining pressure there is no change observed in the drilling rate. They observed that this maximum pressure is different for different rocks. They also showed that not all the rocks behave in the same manner as expected and show different behavior with increasing confining pressure. The rate of penetration decreases significantly at higher weight on bit compared to lower weight on bit. They concluded that drilling rates are greatly affected in the easy-to-drill rocks by change in confining pressure compared to hard-to-drill rocks.

Murray and Cunningham [49] also noticed that drilling rate decreases in impermeable rocks as the confining pressure increase. Experiments conducted on Berea sandstone showed that there was no significant decrease in drilling rate with the increase in confining pressure since it was permeable to the drilling fluid.

Cunningham and Eenink [50] studied the effect of the pressure environment around a bit and conducted laboratory experiments. They observed that the drilling rate is dependent on the difference between the pressure exerted by the mud column and the formation pressure. The drilling rate is independent of mud column pressure if the difference between the mud column pressure and the formation pressure is kept constant. It is observed that rate of change in drilling rate is very high at low differential pressures. As the differential pressure increases, drilling rate reduces.

Cunningham and Eenink [50] also showed that unconsolidated sand is difficult to drill under differential pressure conditions. They understood that the primary reason for the reduction in drilling rates is insufficient cleaning around the bit. The pressure drop across the filter cake does not allow the removal of cuttings. This was verified with the help of increased jet velocities. As the jet velocities were increased, the drilling rates improved significantly. Observation of a drilling experiment on permeable rock with water as drilling fluid prompted them to say that the compression of the rock into its own pores closed the pores or deposition of the cuttings formed an effective filter cake or both possibilities act together. They showed that overburden pressure has no effect on drilling rate if the pressure differential is kept constant and drilling rates decreases with increase in pressure differential.

Discussions by Handin [50], which followed the work of Cunningham and Eenink [50], give a good insight of the cutting process. He agreed with the authors on the fact that the adverse effect of high differential pressure on drilling rate is due to the ineffective cleaning of the cutting from the bottom which results in the entrapment of cuttings and hence recutting of the chips. He added that relative importance of the effects of cutting removal and augmented strength is yet to be ascertained. He hypothesized that if a chip is generated it can only be displaced from its position if drilling fluid has access to these fractures. If the effective pressure is high, the fracture surfaces will be pressed very tightly due to this pressure even if the cohesive strength of the rock has been overcome. At the same time, the void volume increases in a localized zone of failure which results in a local drop of formation pressure, which in turn increases effective confining pressure on the chip. He added that tests on impermeable rocks are required to verify this theory.

Maurer [51] in his study on bit-tooth penetration at different borehole conditions concluded that increase in differential pressure results in the reduction in crater volume in Indiana limestone and Berea sandstone at the same constant force.

Garner [52] studied the cutting action of a single diamond cutter under varying pressure conditions and derived the same results that increasing

the pressure differential between borehole and formation decreases the volume of rock cut by strengthening the rock at constant bit weight.

Vidrine et al. [53] conducted their experiments on shales and concluded that the drilling rate decreases with the increase in differential pressure, but if the formation pressure becomes greater than the mud column pressure, the drilling rate increases. They concluded that by observing the drilling rate, an increase in formation pressure can be detected and this can be used to recognize a kick in the wellbore. At high weight on bit these changes are significant. They also observed that overburden and hydrostatic pressures have no effect on drilling rates and differential pressure between hydrostatic pressure and formation pressure is the only pressure in the affecting the drilling rates.

Garnier et al. [54] worked to determine the effect of chip hold down on the drilling rate. They saturated their rock samples up to the drilling fluid pressure with water. That ensured the zero differential pressure between drilling fluid pressure and pore pressure. During the experiments magnitude of these pressures was varied keeping the difference at zero.

When drilling with water as a drilling fluid, the drilling rate did not change with pressure in the permeable rocks except in the slightly permeable Belgian limestone, which showed a continuous decrease in

the drilling rate with increasing pressure. With water based mud as drilling fluid, the drilling rate decreased in all the rocks with an increase in the pressure. This decrease was limited to a certain pressure. Above this pressure, no change in the drilling rate was observed. For Belgian limestone, both the curves with water and mud overlapped.

Garnier et al. observed that this reduction in drilling rates cannot be explained on the basis of strengthening of rock or by static differential pressure since strengthening occurs at very high pressures, and due to equal mud pressure and pore pressure, there is no static differential pressure.

Garnier et al. explained this phenomenon on the basis of dynamic differential pressure and proposed that after a crack has been initiated, vacuum will be created under the chip unless sufficient liquid is supplied to fill the opening crack. The liquid can be supplied by the means of drilling fluid flowing into the crack, by filtrate flowing through the pores of the chip or by pore liquid flowing through the pores of the rock. Since the initial width of crack is zero and there infinite resistance to flow. If the filter cake is effective filtrate cannot flow to the cracks so pore liquid from the formation is the main supply to fill the opened crack. In nearly impermeable rocks like Belgian limestone, for all practical purpose no liquid is supplied, which leaves the created vacuum under the chip in

place and creating a high pressure difference which force the chip to be held in place. The same phenomenon happens if the rock is permeable, but there is not enough formation pressure to supply the liquid to opened crack. Once the formation pressure rises to a certain value, the differential pressure is created for liquid to flow between formation and the opened crack. Then, the opened crack is filled with liquid. At this pressure, the reduction in drilling rate stops due to continuous supply of liquid in the opened cracks. When drilling with water as drilling fluid, the flow of water through the chip is sufficient to avoid any differential pressure due to a vacuum under the chip and hence no reduction in the drilling rate is seen.

Van Lingen [55] showed that hold down depends on the weight on bit. Hold down increases with increase in weight on bit because of the increase in the length of the path through the crushed zone from the borehole to opened cracks. He also showed that putting the nozzles closer to the formation, the drilling rates can be improved and the reduction in penetration rate can be delayed to a higher weight on bit.

Feenstra et al. [56] experimented on impermeable rocks sample and found out that in the bottomhole conditions where dynamic hold down was present, an increase in nozzle velocity improved the drilling rate. At a low weight on bit, bit balling does not occur so the increase in the

drilling rate is attributed to the reduction in hold down by jetting. This improvement of drilling rate is limited to a certain nozzle velocity and no improvement is seen at increasing high nozzle velocity. Also, no further improvement was seen with the intensification of bottom scavenging by the extension of nozzle to within an inch off the bottom.

Warren et al. [57] proposed that due to the replacement of the weight of overburden rock with mud column, mean stress in the bottomhole reduces significantly. This reduction in mean stress causes an increase in pore volume, and in turn, reduces the local pore pressure in impermeable rock. This causes a differential pressure across the bottomhole even if the wellbore pressure is equal to the pore pressure. This causes the reduction in the drilling rate with depth which is high for impermeable rocks compared to permeable rocks.

Zijsling [58] carried out his experiment on Mancos shale and Pierre shale using a single cutter. He observed that in Mancos shale, the cutting forces are proportional to the total bottomhole pressure and the pore pressure does not have a significant effect on the cutting forces. On the contrary, in Pierre shale cutting forces were found dependent on the pore pressure. Zijsling [58] explained this behavior of the different shale on the basis of dilatancy during the shearing process. This results in an increased pore volume and hence a pore pressure drop due to low

permeability because in Mancos shale, pore fluid from intact rock cannot fill the new extra pore space. When pore pressure drops to cavitation pressure, the shearing process is governed by the total bottomhole pressure rather by pore pressure. In Pierre shale, the dilatancy during the shearing process has a subdued effect due to high porosity and liquids can promptly fill the extra pore space without decreasing the pressure in the pore space.

Gray-Stephens et al. [59] in their work on hard shale observed that the drilling rate was independent of differential pressure and it was dependent on bottomhole pressure.

In the literature, the effect of borehole of pressure condition on different drilling parameter has been studied extensively. Due to recent advances in the mechanical specific energy, it is required to analyze the effect of different borehole pressure conditions on the mechanical specific energy.

CHAPTER IV

SPECIFIC ENERGY IN DRILLING

It is well known, that due to high investment, drilling process is the most important part of the oil and gas industry. Due to its sensitivity to daily oil prices, the drilling process is a crucial candidate for optimization. A small betterment can result in high saving and make the venture a success.

4.1 Properties Used as Drillability Index

In the literature, various parameters have been used to describe the drillability parameter of the rock. Drillability is often termed as a parameter describing the ease of drilling. The parameters used to describe the drillability are not well understood by the petroleum industry. Mostly it comes down to unconfined compressive strength (UCS) and confined compressive strength (CCS) of the rock to define the rock strength during drilling but at the same time it is worth mentioning that different type of rocks like limestone, anhydrite, shale, and sandstone show comparable unconfined compressive strength values, but altogether different behavior during drilling. This means a different set of properties are required to relate drillability of the rocks.

The different rock properties [60] which may be used to describe the easiness of drilling are as follows:

Density
Porosity
Mineralogy
Grain Size
Unconfined Compressive Strength

Density

Density represents the mass per unit volume of the rock. A change in the density can be directly related to the change of the porosity in the rock since it is not affected by the existence of the fractures in the rock. Density of the rock matrix is normally same throughout.

The interpretation of the density is convoluted when the rock matrix is made up of different minerals and is not pure. Also, the presence of gas or different kind of fluids in the pore spaces makes the understanding of the density of the rock a little difficult. If the log data can be refined to remove the above discrepancies to give the actual density, density can be used to calculate UCS and hence CCS of the rock. In most of the cases, it is not the situation and density alone is not used to estimate UCS and CCS properties of the rocks.

Porosity

It is imperative to know the porosity of a rock since it is the measure of the porous space in the rock and causes stress concentration resulting in failure of the rock. A good estimate of the porosity is not available during drilling. The pore volume and its shape and sharpness of edges can be critical to know the strength of the rock. Alignment of cracks and these parameters together can greatly define the strength of the rock if they favor a certain kind of stress concentration.

Mineralogy

Rock characterization, in terms of easiness in drilling, cannot be completed without mentioning the minerals present in the rock. Tool wear and bit balling tendency of a rock can be attributed to the mineralogy of the rock. Commonly found in the rocks of our interest, quartz causes high tool wear due to its hardness and similarly, because of its swelling in presence of moisture, clays cause bit balling. Mineralogy of a rock can be known by the laboratory testing of rock samples and logs.

Grain Size

These properties are reflected in the bulk properties of the rocks such as density and porosity. These properties are often neglected due to the

difficulty in collection and analyzing them in rock samples. Block sizes highlight the brokenness of the rock. Grain sizes vary significantly if the rocks are not crystalline and a representative value is often misleading.

Unconfined Compressive Strength

This is the most understood property of the rock and is considered a fundamental property. It represents the maximum stress that a rock sample can sustain in a uniaxial loading experiment beyond which load carrying capacity drops drastically. It also reflects the energy consumed in the destruction process in a stress-strain plot.

4.2 Mechanical Specific Energy

Mechanical specific energy (MSE) is the energy required to destroy a given volume of the rock during the drilling process. It is stated that in a given drilling environment, lower specific energy depicts a more efficient drilling process. Under atmospheric conditions, when drilling with maximum efficiency, MSE is close to the unconfined compressive strength of the rock [61-62]. MSE is not considered as a fundamental intrinsic property of a rock as it depends on the type of drill bit and bit design. Teale [62] also mentioned that energy spent will become very high if we break the cuttings into “smaller fragments than necessary”. It will

require more particles to be broken without any need and specific energy will significantly increase as the broken particle size is reduced.

MSE can directly be monitored to improve the overall drilling efficiency of the drilling process and detect any changes in the drilling efficiency to optimize the parameter which has caused the deviation.

Specific energy is highly dependent on the equipment used and the nature of rock breakage. Reddish and Yasar [63] presented the parameters on which drilling specific energy depends on:

Rock strength
Rock stiffness
Presence of structural discontinuities
Abrasivity and hardness of the minerals present in the rock
Nature of rock matrix
Nature of mineral grain

In the past, various experimental researches have been made to correlate the drilling efficiency with the known rock properties. Most of the drillability parameters, as discussed earlier, have a major drawback. All the drilling environments have an inherent degree of difficulty in drilling that is only associated to that location or well. No drilling performance parameter takes care of the fact that the drilling situation is totally different in all part of world and there is no correlation between the reservoir properties to benchmark drilling performance.

It is known from the studies that the property that influenced the drilling process most is rock hardness so a particular section takes more time to drill into a hard rock compared to a soft rock. Still we cannot compare the drilling process only on the basis of rock hardness because we know that other factors (like lithology, abrasivity, and borehole pressure) that influence the drilling process are not the same [64]. This means that any comparison just on the basis of drilling time per unit depth is useless if we don't consider the variation in drilling parameters in the soft and hard rock.

Rock strength directly affects the rate of penetration and combined with its easy availability, it is very tempting to use unconfined compressive strength as an index to drillability. It is also known that rate of penetration is also dependent on borehole pressure and in few cases on formation fluid pressure as well. An increase in borehole pressure reduces the rate of penetration in impermeable rock [59, 65]. In the same manner, an increase in difference between borehole pressure and pore pressure reduces rate of penetration in permeable rock.[50, 66]

In the same way, confined compressive strength, has to justify its use as a drillability or performance parameter. The increase in confined compressive strength due to increasing confining pressure is slow as compared to the decrease in rate of penetration due to increase in

confining pressure [54]. Also, the not well known, non linear relationship between increasing confining pressure and compressive strength of rock makes us reluctant to use compressive strength of rock as a drillability parameter.

4.3 Literature Review

Pessier and Fear [67] categorized mechanical specific energy input, drilling efficiency, and a minimum specific energy that is close to rock strength as three key elements of drilling process when looked as a energy-balanced system. They carried out their experiments on grout and Mancos shale under hydraulic pressure. They reported that during the drilling of grout with water as drilling fluid under a bottomhole pressure of 2,000 psi, specific energy was found close to the compressive strength of the grout at the same pressure and mechanical efficiency was found to be 80%. Though specific energy values are almost the double of that observed at atmospheric pressure. Results obtained from Mancos shale shows significant changes at 2000 psi which is drilling with 9.6 ppg lignosulfonate mud. Specific energy values started at 40000 psi and increased up to 80000 psi when experiment has to be terminated due to very high weight on bit (100,000 lbs). A decrease in efficiency from 30% to 20% is observed. Bit balling and bottom balling were observed in the Mancos shale.

They also emphasized that at low depth of cut, specific energy is high and efficiency is low because a minimum has to be reached to start generating cuttings. Below this depth of cut only rock fines are produced.

Caicedo et al. [68] noted that unconfined compressive strength of the rocks can only be used when drilling is done with clear fluids which is hardly the case in any drilling process and also use of confined compressive strength in impermeable rocks is somewhat flawed. They calculated the confined compressive strength of the rock for permeable and impermeable rocks separately. For permeable rocks confined compressive strength is calculated using differential pressure and rock internal angle of friction. Differential pressure is calculated by subtracting pore pressure from equivalent circulation density pressure. For impermeable rocks Skempton model is used to calculate pore pressure in the expanded rock. For a general case effective porosity is used to quantify the permeable and impermeable end points and confined compressive strength is calculated by linearly interpolating the two extreme cases of permeable rock and impermeable rock. A set of correlations are used to calculate rate of penetration and then specific energy, which makes the method unreliable due to accumulated errors of different correlations.

Detournay and Atkinson [69], using the Merchant model for metal cutting, modeled the rock cutting by a PDC bit. They concluded that specific energy of cutting the rock is linearly dependent on the difference between the bottomhole pressure and the average pore pressure on the shear plane. They related pore pressure at the shear plane to the virgin pore pressure by equating the rate of pore volume increase of the rock due to dilatancy and volume of the fluid supplied to the shear plane. They assumed that pore pressure variation in the rock is governed by diffusion.

Detournay and Atkinson [70] defined a parameter λ, on which basis three regimes of drilling can be defined. A value of more than 10 dictates the high speed regime and a value of less than 0.001 dictates a low speed regime. In the high speed regime, rock fails in the shear plane in the undrained manner that means cavitation will occur in the shear plane since there is no change in the fluid content in the pores. Similarly, in the low regime, rock fails in drained manner and the pore pressure in the shear plane and in the intact rock just ahead of the cutter will be almost the same.

Detournay and Atkinson [70] showed that cutting shale is in the high speed regime and pore pressure drop is very high and close to undrained pore pressure drop. This high pore pressure drop causes cavitation. Due

to cavitation specific energy is not dependent on the virgin pore pressure. In a same manner they showed that cutting permeable sandstone is in low speed regime. They concluded that the necessary condition of cavitation is that the rock is shear dilatant and cutting process lies in high pressure regime. Later on, Detournay and Tan [65] showed that in shale, due to cavitation specific energy will only be dependent on bottomhole pressure. They assumed that the inelastic pore volume increase associated with shearing of the rock dominates its volumetric response. They expected that with increase in confining pressure, shear dilatant volumetric strain and inelastic pore volume increase will be progressively reduced and the dilatancy will be eventually suppressed.

Kolle [71] carried out his single cutter experiments under pressure and presented results in terms of drilling strength (indentation load divided by area of cut) and specific energy (tangential load divided by area of cut). In Mancos shale, drilling strength increased with increase in pressure till 25 MPa and after that rate of increase in drilling strength started decreasing. Carthage Marble showed strong effect of pressure on specific energy and drilling strength initially but after 25 MPa there was no significant change. Bonne Terre dolomite exhibited rapid increase in cutter load until 10 MPa but no considerable change beyond that. Colton sandstone showed a rapid increase in drilling strength up to 10 MPa and a more gradual increase thereafter. Berea sandstone exhibited little or no

effect of pressure on drilling strength at low traverse rates due to its relatively high permeability. Kolle [71] could not explain the varying strengthening rates due to high pressure. He presented the theory of dynamic confinement to explain the strengthening of rock with dilation theory.

Judzis et al. [72] conducted full scale laboratory testing on Crab Orchard sandstone, Carthage Marble and Mancos shale. They observed that specific energy in drilling experiments is significantly higher than the compressive strength of the rock at a confining pressure equal to bottomhole pressure. They suspected that other than the work being done due to rock becoming stronger under the confining effect additional unproductive work is also done. This unproductive work may include re-grinding of the cuttings which are held in place on the bottom due to local pressure difference.

4.4 Expressions of MSE

$$MSE = \frac{WOB}{A_B} + \frac{120\,\pi\,N\,T}{A_B\,ROP}$$

where

A_B is bit surface area (in.^{2});

N is rotary speed (RPM);

T is measured torque (lb_f-ft); and

MSE is mechanical specific energy (psi) [73].

Also,

$$MSE = E_m \left(\frac{4 * WOB}{\pi * D^2 * 1000} + \frac{480 * N_b * T}{D^2 * ROP * 1000}\right)$$

where MSE is mechanical specific energy;

E_m is mechanical efficiency;

WOB is weight on bit;

D is bit diameter;

N_b is bit RPM;

T is rotational torque; and

ROP is rate of penetration [74].

4.5 Industry Application of MSE

Generally, a drill rate test [75] is carried out in the field to optimize the rate of penetration (ROP). Different combinations of weight on bit (WOB) and rate of penetration are tested to achieve the optimum rate of penetration. Parameters corresponding to highest ROP are then used to carry out further drilling.

The drilloff test [75] is carried out in the field to see the response of WOB on ROP. After applying a high WOB, the brake is locked. WOB reduces because of further movement of the bit due to continuous drilling. ROP is then calculated from the string elongation data. This data is plotted between ROP and WOB and called a drilloff curve. The point where ROP stops responding to WOB on a linear curve is termed as a flounder or founder point.

The flounder or founder curve gives good insight into the drilling process. At a low WOB, ROP is low due to inadequate depth of cut (DOC). When the DOC is adequate, the ROP responds to WOB in a linear manner and an increase in ROP is proportional to WOB. This is the region where no change in any parameter will cause the ROP to increase since it is already operating in an optimum region. An increase in WOB will simply result in more ROP.

If flounder point does not occur, ROP will increase with the increase in WOB. Flounder point is the condition when energy from a bit to a rock is not properly transferred. In order to increase the ROP at this point, the system needs to be redesigned.

MSE helps us to keep the drilling parameters in check whenever drilling efficiency declines. If the specific energy is close to the confined rock strength of the given environment, the drilling process is efficient and no action is required.

Any deviation in MSE can be tracked to an inefficient parameter in the drilling process. Problems like bit balling, bottomhole balling, string vibration, and bit dulling can be detected very easily and a corrective action can be taken just by looking at the MSE trend.

4.5.1 Bit Selection

Conventionally, bit selection is based on the cost per foot of a drilling process [76], which can be given by:

$$C = \frac{C_B + (T_t + t_r)\, C_R}{F}$$

where, C is cost per foot, C_B is bit cost, C_R is rig cost per hour, T_t and t_r are trip time and rotating time and F is hole section in ft. At every 10 ft, cumulative cost per foot (CCF) is calculated, and when CCF starts

increasing, the bit is pulled out of hole. Few researchers emphasize calculating incremental cost per foot (ICF) for every 10 ft to make a decision on when to pull out a bit.

In this method, rig cost plays a significant role since different rigs will give a different CCF for the same bit.

Specific energy for the rotary drilling is given by Moore [77]

$$E_s = \frac{20\,W\,N}{d\,R_P} = \frac{20\,W\,N}{d\,F}\,t_r$$

where, W is weight on bit, N is rotary RPM, d is diameter of bit, R_P is rate of penetration, F is drilled footage and, t_r is rotating time.

Since E_s is highly dependent on bit type and design, specific energy can be taken as a bit selection criterion. The fact that for a formation of given strength a hard formation bit will give a totally different set of E_s as compared to the soft formation bit, supports the idea.

In the above equation, it is clear that for a given bit type, E_s can be considered constant for different WN values since change in WN leads to change in R_P. At the same time, ROP is highly sensitive to change in WN values. This dictates that E_s can be used as a direct measure of bit performance and, due to less sensitivity to WN as compared to penetration rate, is a good tool for bit selection.

Abdollahi et al. [78] proposed to select a bit on the basis of benchmarked bit. A bit which gives minimum MSE is preferred to drill a particular formation of interest and on the same basis bits can be changed in different formation streaks to give better efficiency in drilling process.

4.5.2 Benchmarking of Drilling Process

With the help of the tool at hand, the most obvious thing to be done with the drilling process is benchmarking it with global conditions. In the past, it does not seem wise because of several differentiating conditions in the drilling environment. MSE, as long as the same bits are being used, can help with that by benchmarking the drilling process regarding energy required to drill the formation. For different bits in the same environment, it is easier to pick the most efficient bit on the basis of less MSE required. Different bits can be run in a particular formation and the one with the least MSE can be benchmarked for the future use. The major drawback might be the case where bit with best efficiency is yet to make a run in the formation and no data is available for benchmarking [78].

Abdollahi et al. [78] showed that taking time into consideration while optimizing the whole drilling process better results can be achieved for benchmarking.

4.5.3 Dull Bit Evaluation and Deciding on Pulling Out a Bit

Abdollahi et al. [78] mentioned that to know the condition of a running bit, a better understanding of incremental bit wear on the different drilling conditions is required. ROP and other common drilling parameters can not conclusively tell us that the low efficiency of the drilling process is due to dull bit. Also, the peaks in these logs show several plots and it is difficult to recognize which peak is caused by dull bit.

Using Abdollahi's minimum energy concept, minimum energy should have a constant slope when plotted against measured depth pertaining to the conditions of a new bit and homogeneous formation. It was shown that the slope of this curve gives a better understanding on deciding on when to pull out a dull bit. When minimum energy approaches a horizontal asymptote, which means a decreasing efficiency coupled with the cost per foot of the drilling, a decision on when to pull out a bit can be made.

4.5.4 Bit Balling

Bit balling [75] can be defined as a situation in which transfer of energy from the bit to the rock is hampered by the accumulation of material within the cutting structure. A reasonable drilling rate and a high

specific energy jump can be seen because of bit balling. A bit with identical features and a better Hsi can be lowered to enable cleaning. Better hydraulics does not eliminate bit balling but it extends the flounder point so that bit balling occurs at higher WOB and ROP.

CHAPTER V

EXPERIMENTAL SET UP

5.1 MICROBIT Simulator

A 'MICROBIT' Simulator, provided by Baker Hughes, is a high pressure drilling simulator which is designed to test drilling performances of micro-bits in various rocks and drilling fluids.

MICROBIT simulator [79] is an extraordinary simulator since it can simulate the high pressure of a reservoir while drilling a sample of rock. MICROBIT simulator consists of all the required equipments needed for a drilling operation, including: desktop controls through LabVIEW program 'MICROBIT', a high pressure triplex pump, a drill stem rotary, and an intensifier to pressurize the rock chamber. The following are the main systems of the MICROBIT simulator:

Rotary System,
Mud System,
Pressure Intensification System,
Rock Movement System,
Analog Electrical System,
Data Acquisition System,

5.1.1 Rotary System

This system is powered by an AC motor controller. The rotary speed is entered manually to minimize the feedback noise. This controller powers a 7 ½ HP three phase electric motor. The output shaft of the motor is connected to a 10: 1 speed reducer, where after, a torque load cell and a rubber lined coupling are fixed. The shaft then enters to the pressure vessel base and rotates the drill stem by using a 90° bevel gear. A rotary seal is placed from where the drill stem runs through the pressure vessel to where the bit is screwed on at the end.

5.1.2 Mud System

There are two mud tanks available, whose capacities are 30 and 100 gallons. Both of the tanks are connected to a header situated underneath by multiple valves. This header is connected to a 1 in. diaphragm pump from which flow can be diverted either inside to a micro-bit or back to either of the tanks.

If the flow is directed into a micro-bit, a set of three large 'Weco' valves is encountered. In-flow passes through the bottom valve and can be diverted to the high pressure triplex pump. The flow enters to the input header of the pump and to the check valves. The flow is then pulled by the retraction of cylinders and pushed out to discharge manifold. From

this manifold, the flow goes through a borehole pressure transducer and finally enters into the pressure vessel. When it enters the pressure vessel, it passes through the rotary seal and into the annulus of the drill stem and comes out through the micro-bit. After flowing back around the bit, it goes down through a hole, which is located on the side of the pressure vessel. It flows past the borehole pressure transducer and goes into the side of the filter vessel. This filter consists of a cylindrically shaped wire mesh. From the filter, flow goes to a four way junction.

If the middle left large valve is closed and the top large Weco valve is open, the flow will pass through the pipes and go back to the tanks. This creates an 'Open Loop System'. Similarly, if the middle left large Weco valve is open and the top large Weco valve is closed, the flow will enter to the pipe that is supplying the flow to duplex pump. This forms a 'Closed Loop System'.

A small, high pressure ball valve is located on the corner of the MICROBIT simulator, which is also just above the rupture disk. If this valve is open, the flow will be directed to a ¼ in. high pressure tube and will go into the return line downstream of the large Weco valves, which finally directs the flow to mud tanks. If the pressure in the line exceeds 11,250 psi, it will blow the rupture disk to the left and lead the flow to the pressure relief pipe described earlier. The flow will be directed to the

mud tanks. Another small, high pressure valve is placed on the top of the pressure vessel. It is only opened when the simulator is in the open loop or semi-open loop configuration to allow any trapped air in the system to escape.

5.1.3 Pressure Intensification System

MICROBIT simulator is pressurized by a plunger type intensifier, which is fed by an air over water cylinder placed at the backside of simulator. The inlet check valve on the intensifier is supplied with 90 psi of positive pressure by the air. When the plunger of the intensifier retracts, water is sucked in through the inlet check valves and when the plunger extends water is pushed out through the outlet check valves. This water runs through a tube into a port on the side of the filter vessel. As more and more water is pushed into the system, the pressure rises to the set pressure. This high pressure is released by opening the small pressure ball valve located on the corner of the simulator, which is just above the rupture disk.

It is important to note that pressure in the MICROBIT simulator can only be increased when system is in closed loop configuration and all the trapped air has been bled from the system.

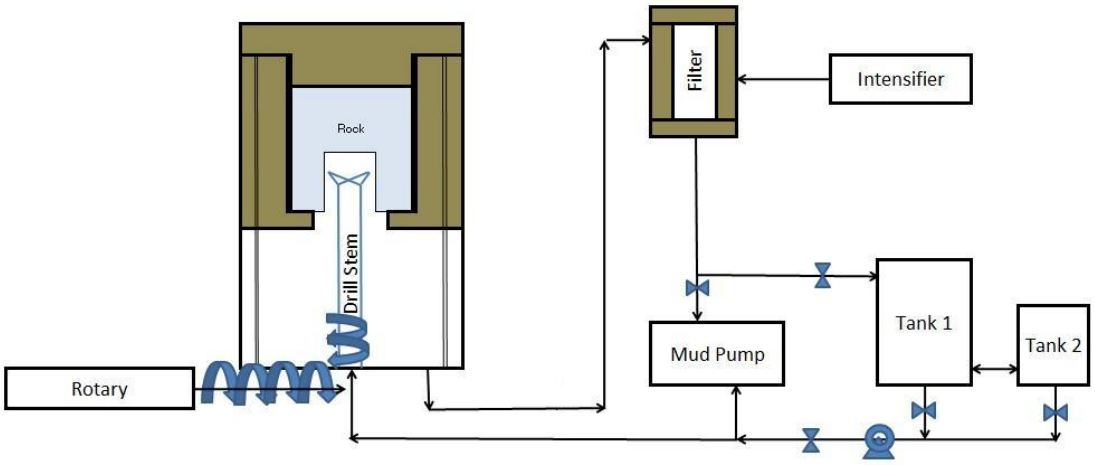

Fig. 5.1: Schematic of drilling experiment set up

5.1.4 Rock Movement System

At the start of the experiment, a rock is held in the pressure vessel by the rock holder, which is at that time, positioned above the drill stem. Two ¼ in. long stainless steel rods run from the sides of the rock holder, down through the bottom of the pressure vessel, and finally into two load cells mounted on a metal bar. These two stainless steel rods are responsible for moving the rock holder up and down. The rod end of an inverted hydraulic cylinder is connected to the metal bar. As the hydraulic cylinder extends, the rock moves down closer to the bit. Similarly, as the cylinder retracts, the rock moves up and further away from the bit (see **Fig. 5.2**). The applied pressure to the hydraulic cylinder is controlled by a servo controller. A depth meter is also attached to the metal bar

containing the load cells which explains that the rock holder can be moved up or down by controlling weight on bit (WOB) or the depth.

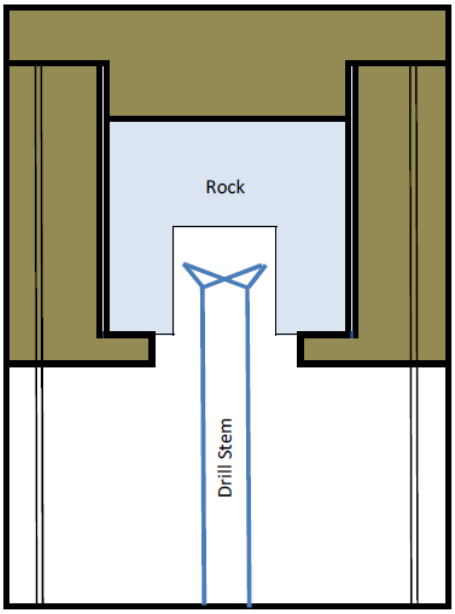

Fig. 5.2: Schematic of rock holder

5.1.5 Analog Electrical System

Four analog signals handled by the "MICROBIT" program are torque, weight on bit (WOB), bottomhole pressure (BHP), and supply pressure. The servo valve that controls the hydraulic cylinder, responsible for moving the rock holder, is controlled by a factory assembled circuit board, called a Moog card. This card supplies a setpoint voltage and feedback voltage. This can either be weight on bit (WOB) setpoint and feedback signals or rate of penetration (ROP) setpoint and feedback signals. Based on what signals are being sent to the Moog card, it is

either functioning as a WOB controller or as a ROP controller. When the relay which decides which signal to send to the Moog card is off, the card is sent a WOB feedback signal. If that relay is on, then the card is sent a rate of penetration feedback signal.

5.1.6 Data Acquisition System

LabVIEW is the computer programming language which has been used to record and control the MICROBIT simulator, via a program called "MICROBIT". Inside the controlling computer, a circuit board called the LabVIEW MIO 16X Card (multiplexing input and output) has been installed. With the help of this card, LabVIEW can record analog input signals and send analog and digital output signals.

5.2 MICROBIT User Interface

It is important to understand what the MICROBIT interface offers to its user. **Fig. 5.3** shows the initial start up screen of the MICROBIT program. BHP setpoint and WOB setpoint are kept at -100 lb_f and -15 psi. The reason for this is to avoid the hydraulics and servo running accidentally, at the start of program.

WOB, Torque, BHP, RPM, and ROP are the real time values of weight on bit, torque, bottomhole pressure, rotary revolution per minute and, rate

of penetration of the bit. BHP setpoint and WOB setpoint are the desired input values of bottomhole pressure and weight on bit.

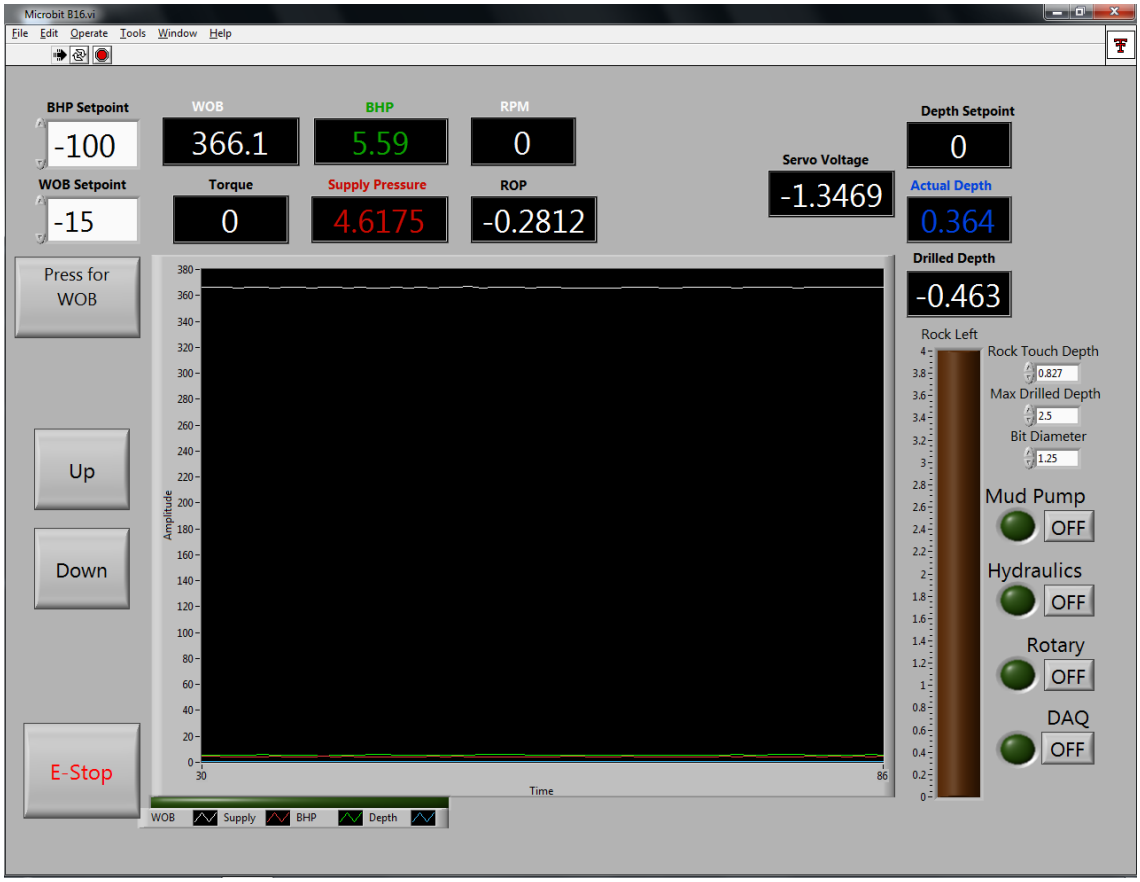

Fig. 5.3: User interface of MICROBIT program

Supply pressure is the pressure which is supplied by the intensifier, to keep the real time bottomhole pressure close to setpoint pressure. Servo voltage is a critical parameter to control the hydraulics. A high value of Servo on either side of zero means that the hydraulics is trying to move the bit in either direction. A value of Servo, in the Servo voltage field, of more than 0.1 is alarming and should be controlled carefully.

At the right hand corner of the screen, depth setpoint is the user-provided desired depth, while actual depth is the real time depth of the bit. A difference in these values defines the Servo activity, and Servo voltage can be controlled by altering these values. Also, if we provide the rock touch depth, it will give us the actual drilled depth, given that drilled depth is the depth drilled by the bit at any time. It is important to note that the reference for the depth is the top position of the rock holder, labeled zero.

Controls for the mud pump, hydraulics, and rotary are placed at the bottom, on the right side of the screen. To collect the data, the DAQ (data acquisition) tab has been provided to start recording the data and save the file at any given location of the user's preference.

Initially, the rock is touched when the program is on *depth control mode*. The up and down tabs are used to move the rock holder up and down. When the rock touches the bit, a significant increase in the WOB can be observed; and from that point onwards, the program can be turned to *WOB mode* to keep a constant WOB on the rock. A tab has been provided to stop the MICROBIT simulator, in case of an emergency.

5.3 Rock Samples and Properties of Rock Sample

Samples of the rock are prepared in the manner of which to be used within the rock holder. Diameter of the rock sample is approximately 4 in. and the length of the sample is 3 ¾ in.

Two types of rocks are used in the experiments: Carthage Marble and Crab Orchard. Properties of these two rocks are summarized below in **Table 5.1**:

Table 5.1: Properties of Carthage Marble and Crab Orchard

Property	Carthage Marble	Crab Orchard
Density (g/cc)	2.62	2.53
Porosity (%)	1.7	2
Unconfined compressive Strength (ksi)	13	24.3
Permeability (md)	0.002	0.1
Sonic (P)	19569	9480
Sonic (S)	10695	4750
Friction angle	32.2	52.3
Cohesion (psi)	4750	7300

5.4 Steps Followed During the Experiments

Since the system involves high pressures and heavy fitting it is highly recommended to work in a safe condition. Due care was taken to avoid any situation which could lead to an accident. These are the following steps which were followed during the experiments.

1. Turn Power "ON" at the main switch box.
2. Mix and check the mud to be tested.
3. Prepare the rock.
4. Assemble the rock holder.
5. Open the MICROBIT program.
6. As soon as the program starts, the hydraulics starts with it. Check WOB (-15 lbs) and BHP (-100 psi). Check the Servo voltage; it should be close to zero.
7. Check the Mud Flow Configuration. It should be in 'Open Loop Configuration' as follows:

   Supply Valve: OPEN
   Return Valve: OPEN
   HP#2 Valve: CLOSE

   At the same time,

   Upper Air Bleeder Valve: CLOSE
   Pressure Relief Valve: CLOSE
8. Fill the air/water cylinder with water.
9. Open the mud tank supply.

10. Start transfer pump at the mud tank.
11. Bleed air from the Upper Air Bleeder Valve to make sure the pump is pumping water in the system.
12. Turn “ON” the mud pump.
13. Open the air to the air/water cylinder.
14. Change to ‘Semi Open Loop Configuration’ by operating the following valves in the given sequence:

    HP#2 Valve: OPEN
    Return Valve: CLOSE

15. Bleed the air from the Upper Air Bleeder Valve.
16. Change to ‘Close Loop Configuration’ by closing the supply valve.
17. Start the rotary.
18. Pressurize the system by entering the BHP setpoint and hitting the enter key.
19. When pressure stabilizes, SWITCH ON the DAQ.
20. Change the WOB to a positive value (as required and planned).
21. Touch the rock slowly by pressing the down button and keeping an eye on WOB. (Note the rock touch depth and enter it in the given column.)
22. Switch to *WOB mode* immediately after touching the rock.
23. Continue drilling until;

    Drilling Depth = rock touch depth + required length of hole.

24. STOP hydraulics.

25. STOP DAQ.

26. Turn “OFF” the mud pump.

27. Release the pressure from the Upper Air Bleeder Valve. (Set the BHP to -100).

28. STOP the rotary.

29. Change to ‘Open Loop Configuration’.

    Supply Valve: OPEN
    Return Valve: OPEN
    HP#2 Valve: CLOSE

30. Purge air.

31. Take the rock out from the rock holder.

32. Set hydraulics back to *Depth Control mode*.

CHAPTER VI

RESULTS AND DISCUSSIONS

Experiments on Carthage Marble and Crab Orchard sandstone samples were carried out at constant operational parameters (Weight on Bit (WOB), Rotation per minute (RPM) and flow rate) and different confining pressure of 250 psi, 500 psi, and 1,000 psi. All the experimental results were analyzed for mechanical specific energy (MSE), rate of penetration (ROP), and cutting force on the basis of either depth or depth of cut (DOC).

Carthage Marble and Crab Orchard were investigated separately and the effect of confinement on the mechanical specific energy and other drilling parameters was the focus of analysis.

Fig. 6.1 shows the variation in the mechanical specific energy for Carthage Marble at different pressure with depth of drilling. It is noted that the MSE at 250 psi is at minimum while the MSE at 1,000 psi shows the highest peaks. The MSE plot for 500 psi lies in between plots for 250 psi and 1,000 psi.

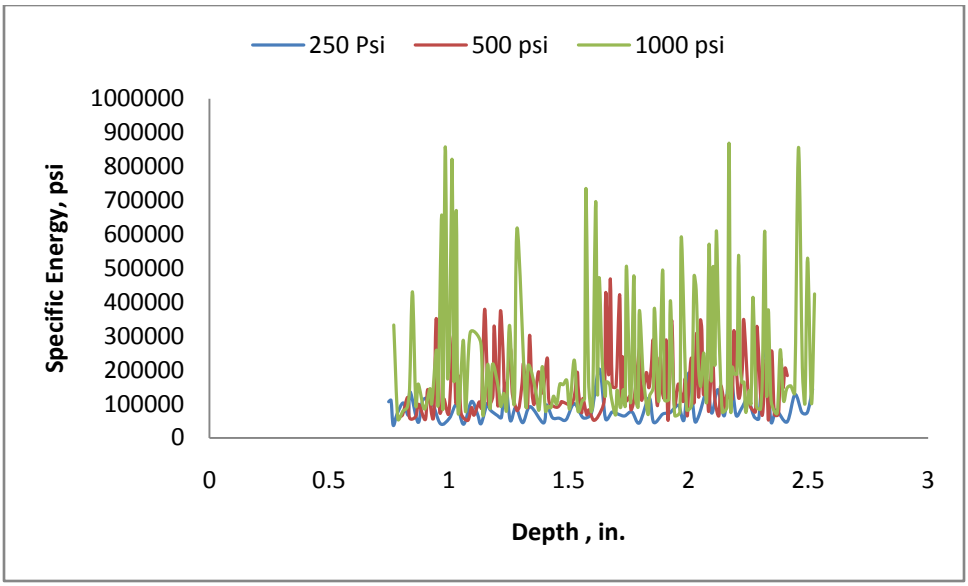

Fig. 6.1: Change in specific energy with depth for Carthage Marble at different pressures

As mentioned in previous investigations, the strength of the rock increases with the increase in confinement pressure, so the increase in the MSE values was keeping the trend.

A high fluctuation in the values can be explained due to the brittle nature of the rock and hence the random breakage of the bond between grains. Also, it is important to mention that the servo mechanism responsible to maintain a constant WOB is an “on and off” mechanism; this inertia of the servo control may be one of the causes for this very high fluctuation in MSE. Moreover, the elasticity of the drill stem can also be held responsible due to its tendency to hinder the transmission of power to the bit. In this case, because of the small length of the drill stem, this effect can be ignored.

A similar graph for Crab Orchard is shown in **Fig. 6.2**.

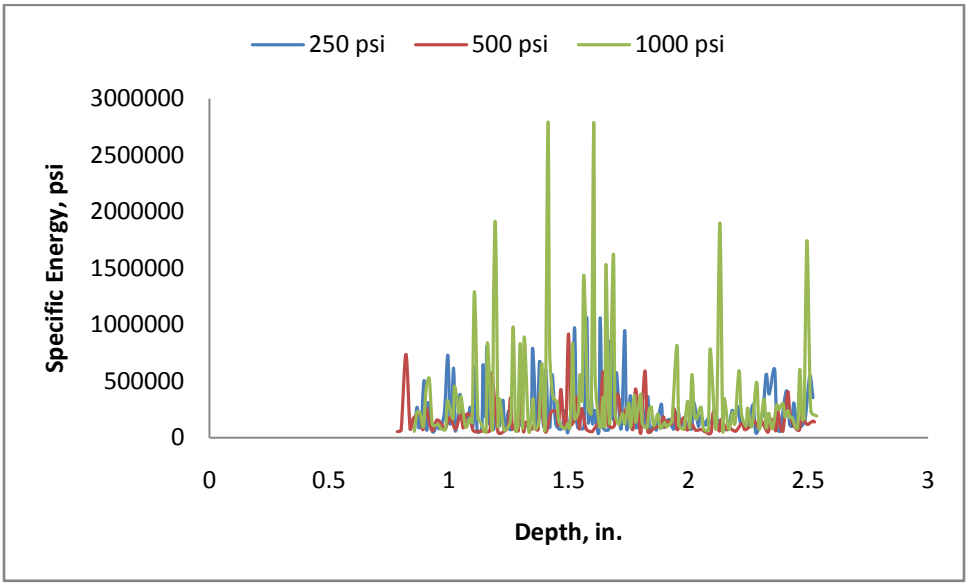

Fig. 6.2: Change in specific energy with depth for Crab Orchard at different pressures

The results show the higher peaks in the MSE values for Crab Orchard, being harder of the two rock types.

As the DOC and WOB were not constant during the drilling experiments, it was possible to analyze the variations in the MSE with respect to the changes in the DOC. **Fig. 6.3** shows a good relationship of the mechanical specific energy with the depth of cut for Carthage Marble with a coefficient of correlation more than 0.8 in all the cases.

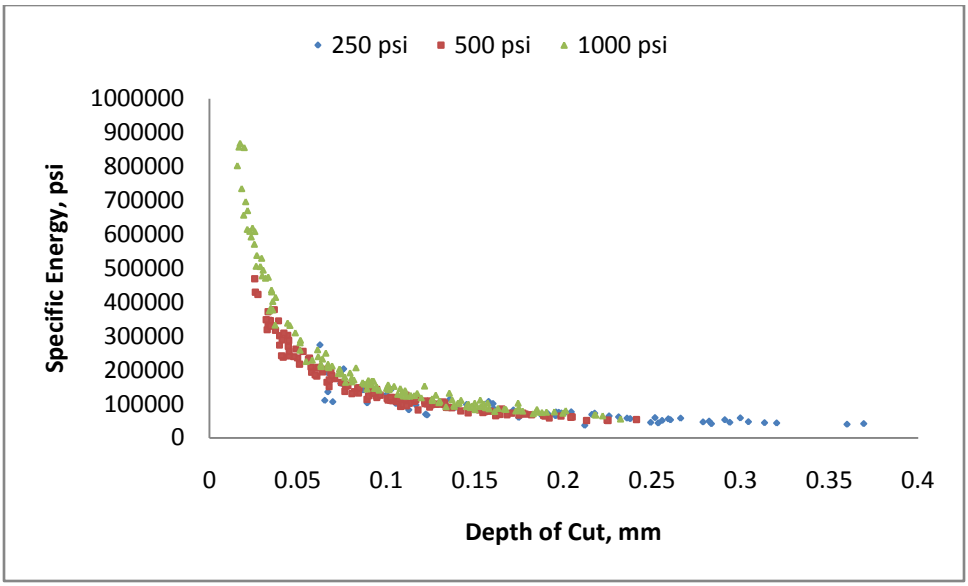

Fig. 6.3: Change in specific energy with DOC for Carthage Marble at different pressures

Also, for the same DOC, MSE is the highest at 1,000 psi and the lowest for 250 psi. MSE is very high at low DOC, which indicates that the drilling process is very inefficient resulting from friction or grinding rather than cutting. From the above results, it is possible to conclude that the changes in the DOC were caused by the changes in the WOB.

One interesting note worth mentioning at this point is that the minimum DOC for all the confining pressure is different in all of the cases (see **Table 6.1**). At the same target value of WOB, minimum and maximum DOC for 250 psi is highest while it is lowest for 1,000 psi. That implies that the same rock is more difficult to drill when under a higher confinement pressure.

Table 6.1: Minimum depth of cut observed during the experiments at different pressures

Pressure (psi)	Minimum DOC for Carthage Marble (mm)	Minimum DOC for Crab Orchard (mm)
250	0.06	0.01
500	0.05	0.01
1,000	0.05	0.005

Also, as the DOC increases, MSE reduces and the drilling process becomes more efficient (see **Table 6.2**). It is believed that as the DOC increases, MSE achieves even a lower value and tends to be equal to the confined compressive strength of the rock at optimum DOC.

Table 6.2: Maximum DOC and corresponding minimum specific energy at different pressures

Pressure (psi)	Carthage Marble		Crab Orchard	
	Max DOC (mm)	Min SE (psi)	Max DOC (mm)	Min SE (psi)
250	0.37	37161	0.20	65177
500	0.24	51310	0.21	56598
1,000	0.23	55348	0.23	70572

Fig. 6.4 shows the relationship between the mechanical specific energy and the depth of cut for Crab Orchard at different confinement pressures.

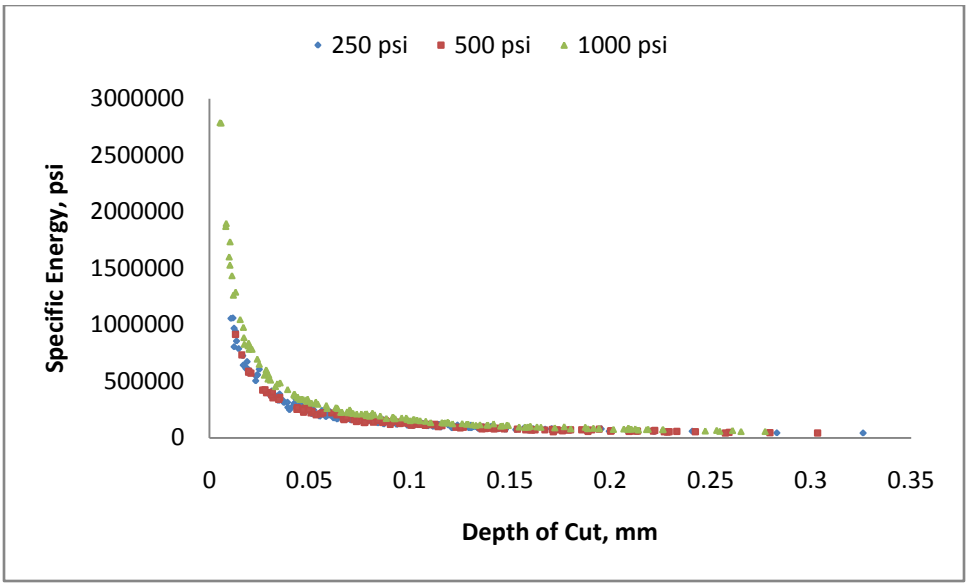

Fig. 6.4: Change in specific energy with DOC for Crab Orchard at different pressures

At 1,000 psi, Crab Orchard shows a significant increase in MSE values from 500 psi to 1,000 psi compared to 500 psi from 250 psi. The results indicate that the stronger rock, Crab Orchard (UCS=24,300 psi) is sensitive to changes in confinement pressure at higher values of this pressure compared to the weaker Carthage Marble (UCS=13,000 psi).

Efforts were also made to compare two rock types, having different characteristics, to see how they reacted to the confining pressure.

Fig. 6.5, **Fig. 6.6**, and **Fig. 6.7** show the relationship between the mechanical specific energy and the depth of drilling for Carthage Marble and Crab Orchard at 250 psi, 500 psi, and 1,000 psi, respectively.

It is seen that in all the cases, MSE is quite higher for Crab Orchard, having a higher UCS than Carthage Marble. At 1,000 psi, Crab Orchard shows a drastic change in the MSE compared to Carthage Marble.

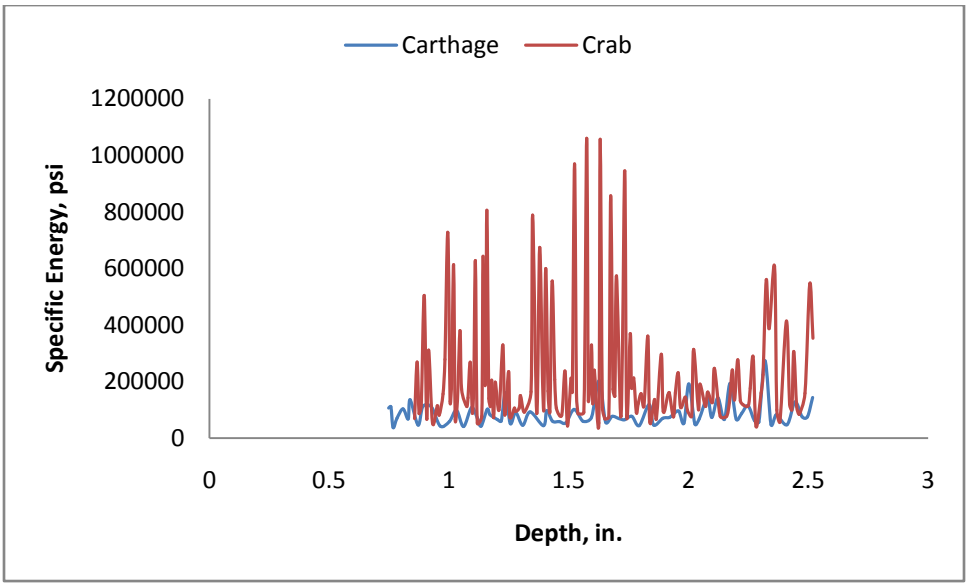

Fig. 6.5: Specific energy vs. depth for Carthage Marble and Crab Orchard at 250 psi

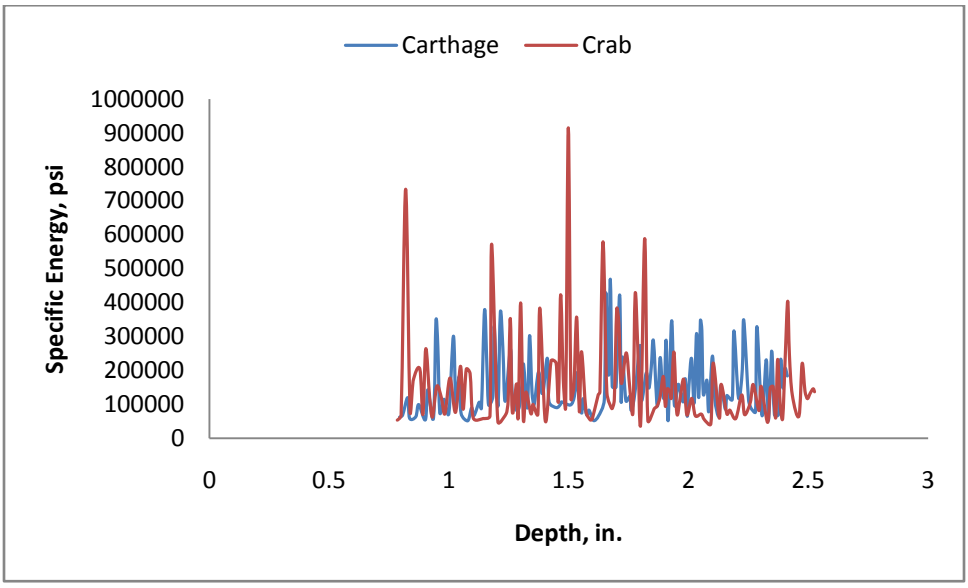

Fig. 6.6: Specific energy vs. depth for Carthage Marble and Crab Orchard at 500 psi

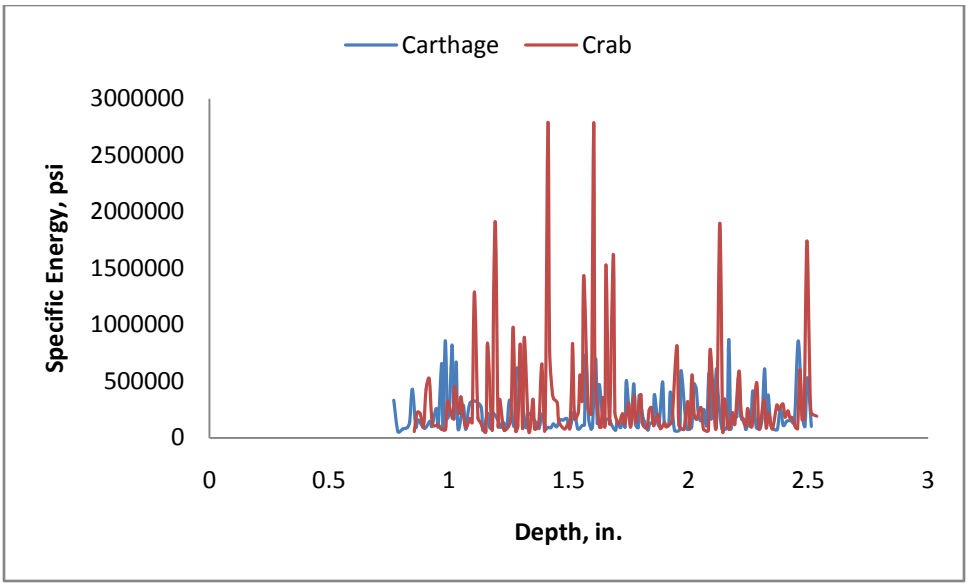

Fig. 6.7: Specific energy vs. depth for Carthage Marble and Crab Orchard at 1,000 psi

Fig. 6.8, **Fig. 6.9**, and **Fig. 6.10** show the behavior of the mechanical specific energy due to the change in the depth of cut. Being the harder of the two rocks and as previously discussed, at the same DOC, Crab Orchard shows higher MSE at all the pressures as compared to Carthage Marble. This change is significant for the pressure change from 500 psi to 1,000 psi.

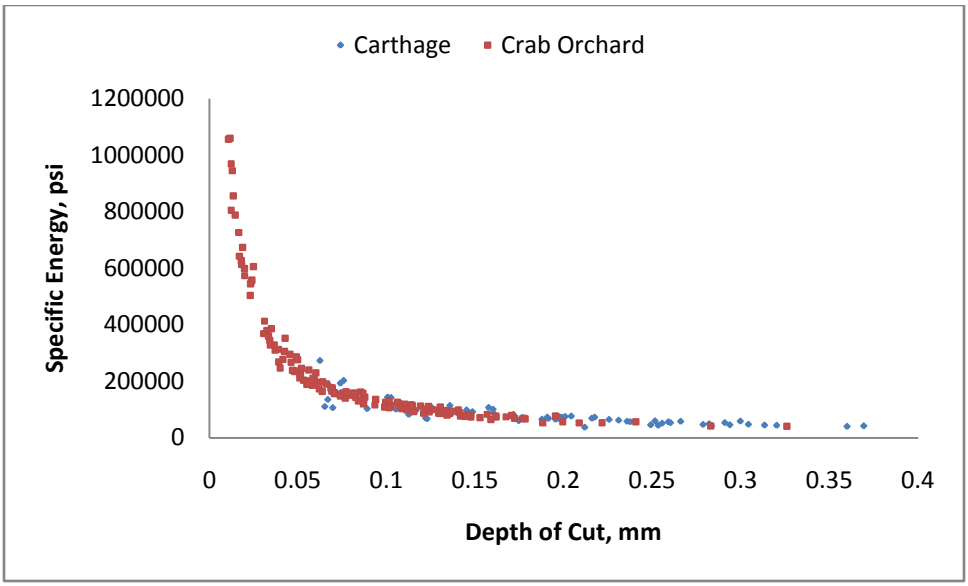

Fig. 6.8: Specific energy vs. DOC for Carthage Marble and Crab Orchard at 250 psi

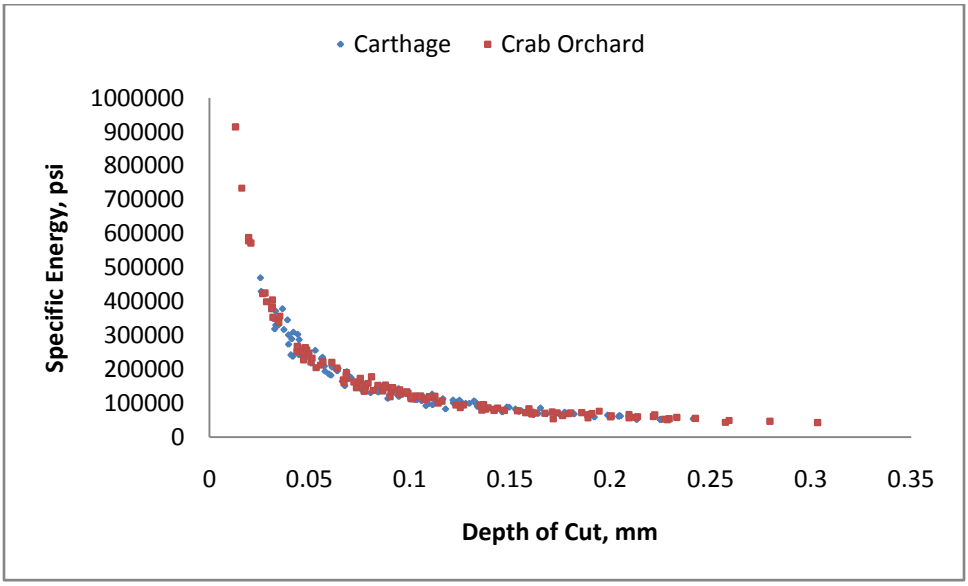

Fig. 6.9: Specific energy vs. DOC for Carthage Marble and Crab Orchard at 500 psi

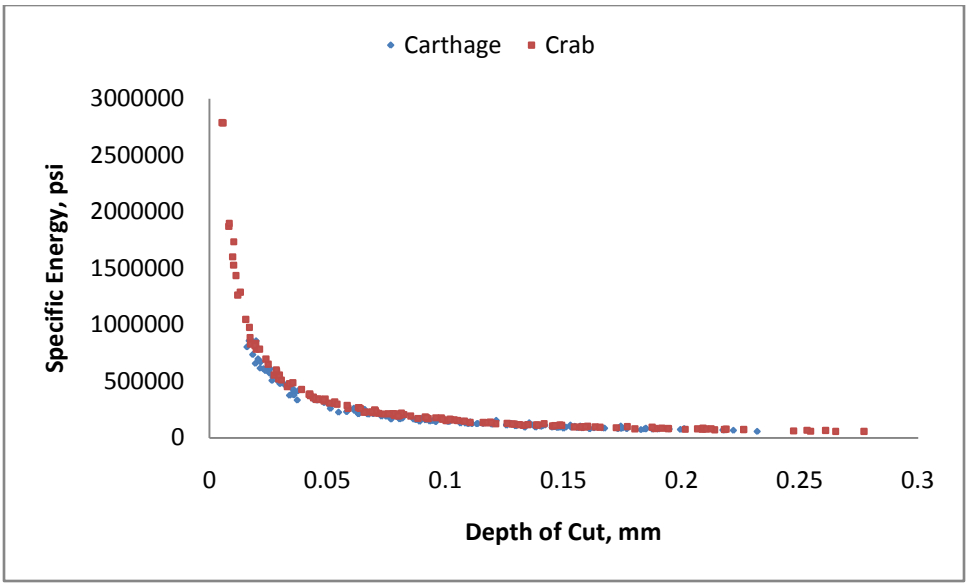

Fig. 6.10: Specific energy vs. DOC for Carthage Marble and Crab Orchard at 1,000 psi

Fig. 6.11 shows a relationship between the rate of penetration and the depth of cut at different confining pressures for Carthage Marble.

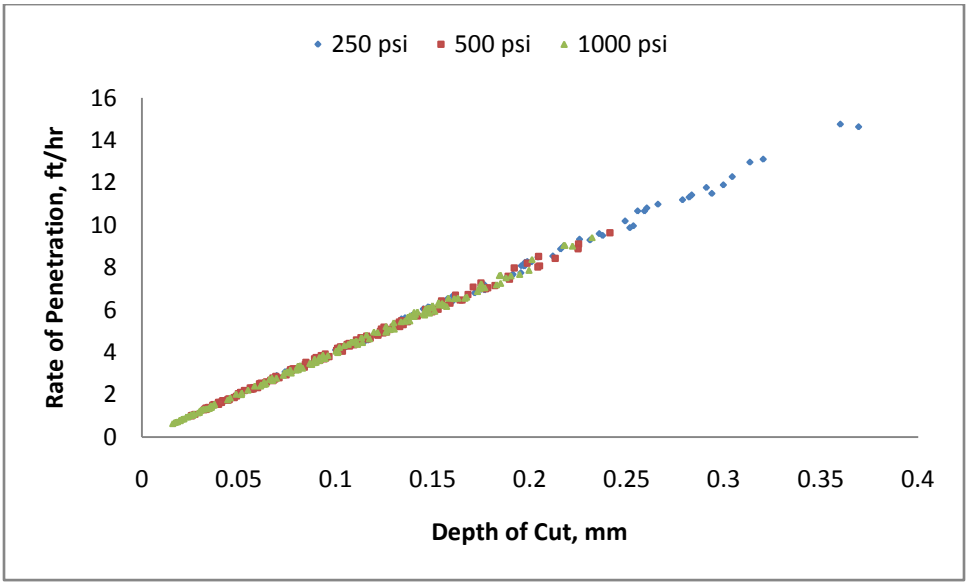

Fig. 6.11: ROP vs. DOC for Carthage Marble at different pressures

Consequently, due to high effective differential pressure, the ROP at 1,000 psi is lower when compared to the ROP at 250 psi and 500 psi.

Fig. 6.12 shows a similar relationship between the rate of penetration and the depth of cut at three different confinement pressures for Crab Orchard.

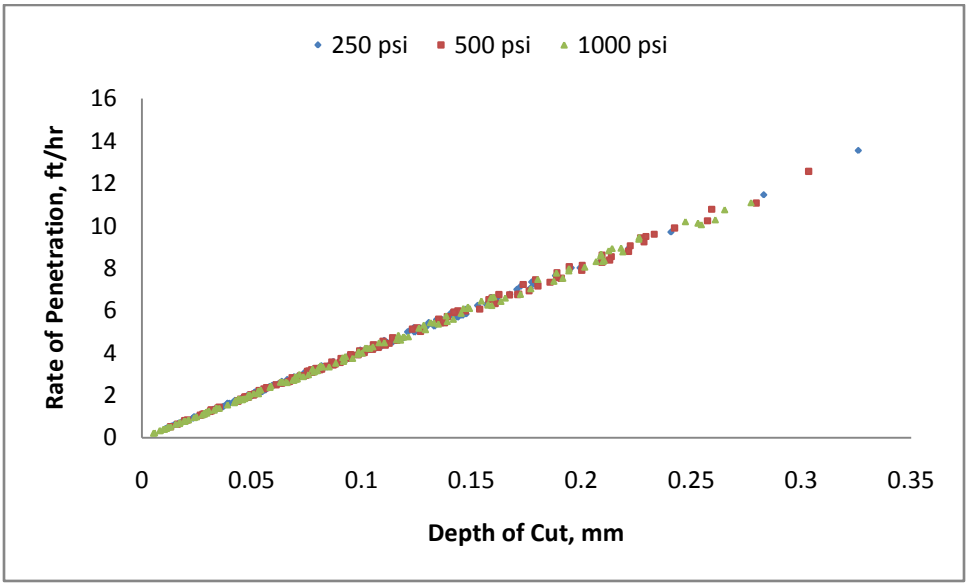

Fig: 6.12: ROP vs. DOC for Crab Orchard at different pressures

The rate of penetration of the two rocks at different confining pressure is compared and plotted against the depth of cut. **Fig. 6.13**, **Fig. 6.14**, and **Fig. 6.15** show these relationships between rates of penetration.

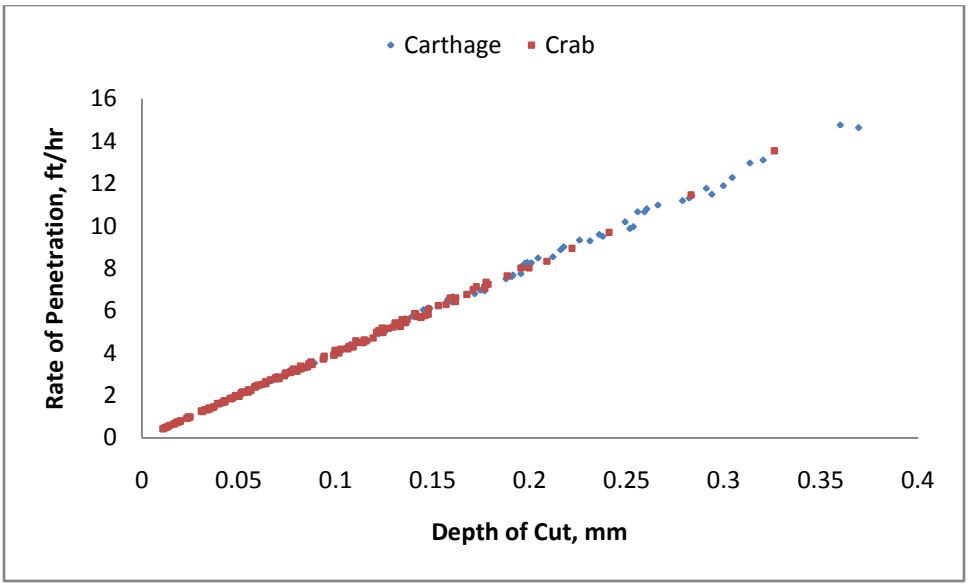

Fig. 6.13: ROP vs. DOC for Carthage Marble and Crab Orchard at 250 psi

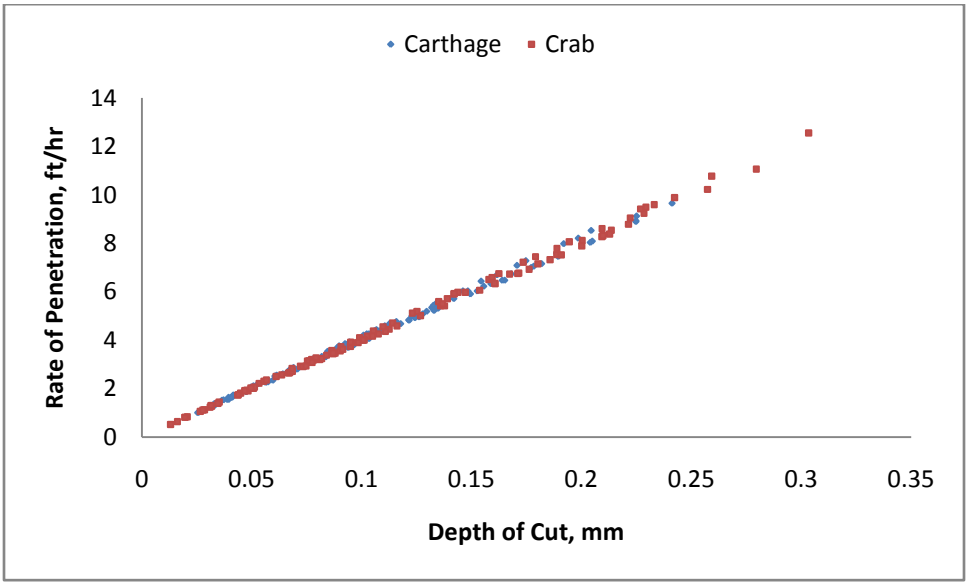

Fig. 6.14: ROP vs. DOC for Carthage Marble and Crab Orchard at 500 psi

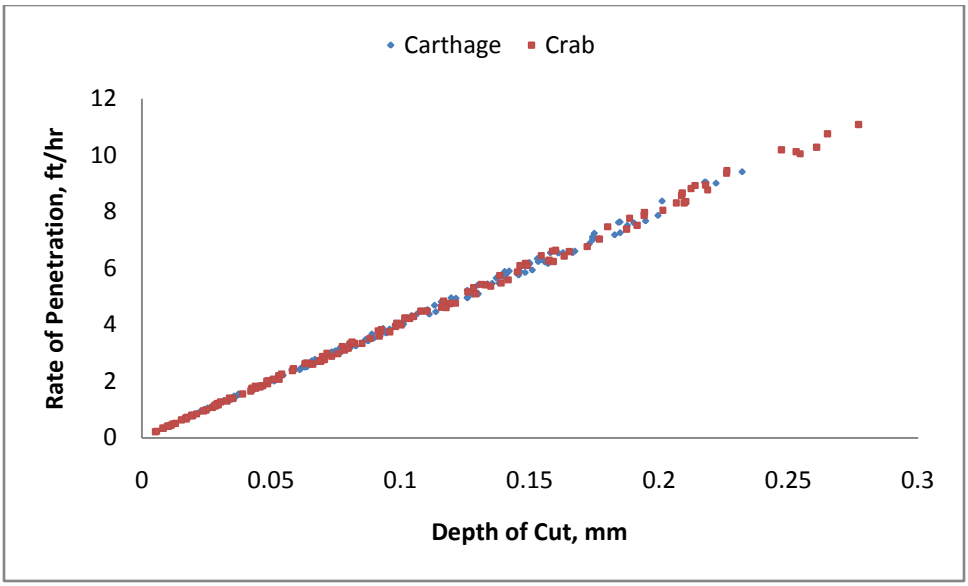

Fig. 6.15: ROP vs. DOC for Carthage Marble and Crab Orchard at 1,000 psi

At first it seems surprising to see the approximately same ROP for both the rocks, but a closer look at the permeability of the rocks clarifies the issue. A difference in the ROP on the basis of differential pressure created by the relative higher permeability of Crab Orchard is expected, but at the given permeability for both the rock, drilling fluid (being water) cannot permeate the rock in front of the cutter and negates any effect due to permeability. The high strength, high permeability of the Crab Orchard and the low strength, low permeability of the Carthage Marble coupled with low DOC make it difficult to conclude any results on the basis of Fig. 6.13, Fig. 6.14, and Fig. 6.15.

Fig. 6.16 and **Fig. 6.17** show the relationship between the cutting force and the depth of cut for Carthage Marble and Crab Orchard, respectively.

In Fig. 6.16, it is seen that as the confining pressure goes from 500 psi to 1,000 psi there is a distinct change in cutting force values. Data for 250 psi is scattered due to the high fluctuation, but it helps to recognize that as the DOC increases the cutting force also increases.

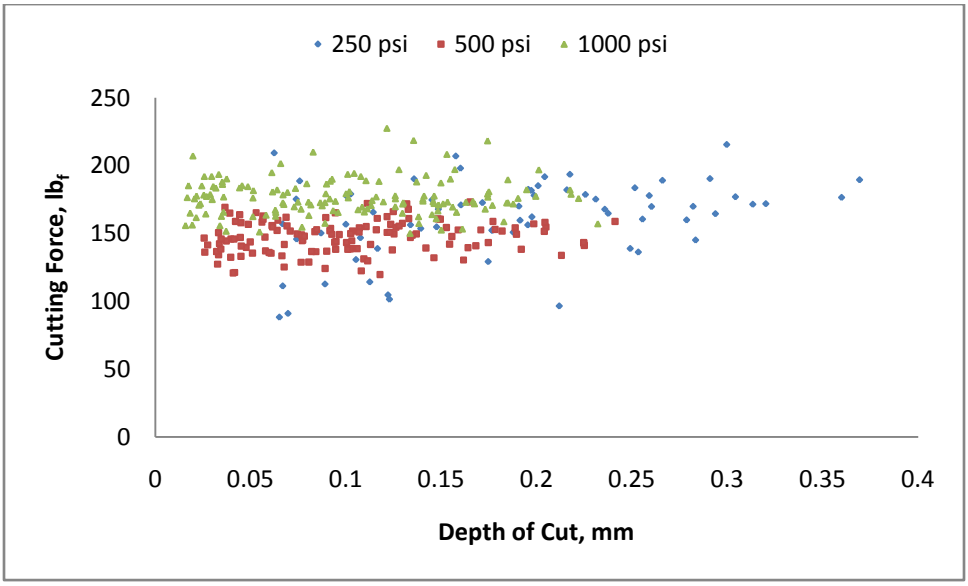

Fig. 6.16: Cutting force vs. DOC for Carthage Marble at different pressure

Similarly, Fig. 6.17 shows that going from the 250 psi to 500 psi, cutting force values do not change much but there is a significant change in cutting force from 500 psi to 1,000 psi.

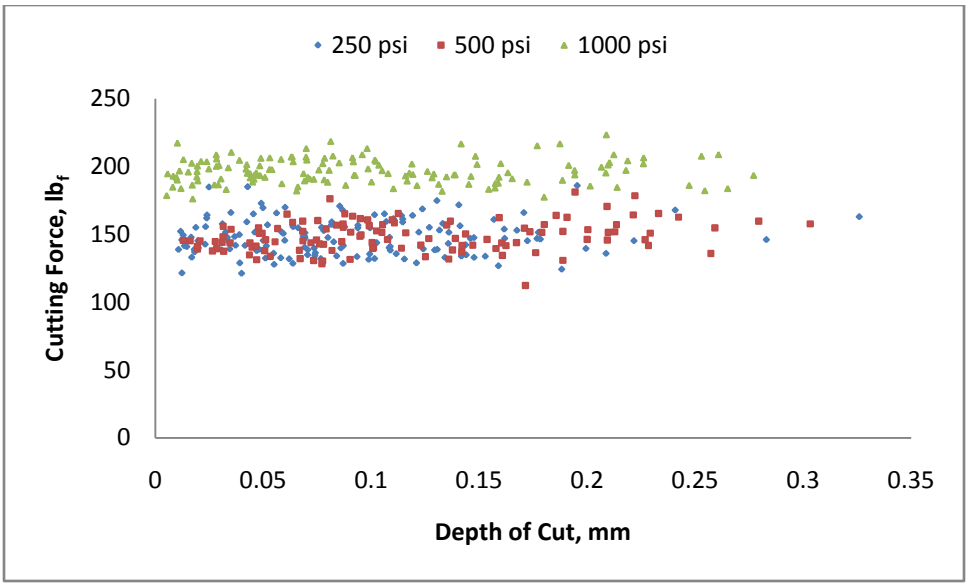

Fig. 6.17: Cutting force vs. DOC for Crab Orchard at different pressure

It can also be inferred that Carthage Marble responds gradually to confining pressure change, while Crab Orchard shows significant changes above 250 psi.

Fig. 6.18, **Fig. 6.19**, and **Fig. 6.20** show the relationship between the cutting force and the depth of cut at 250 psi, 500 psi, and 1,000 psi respectively for both the rock types.

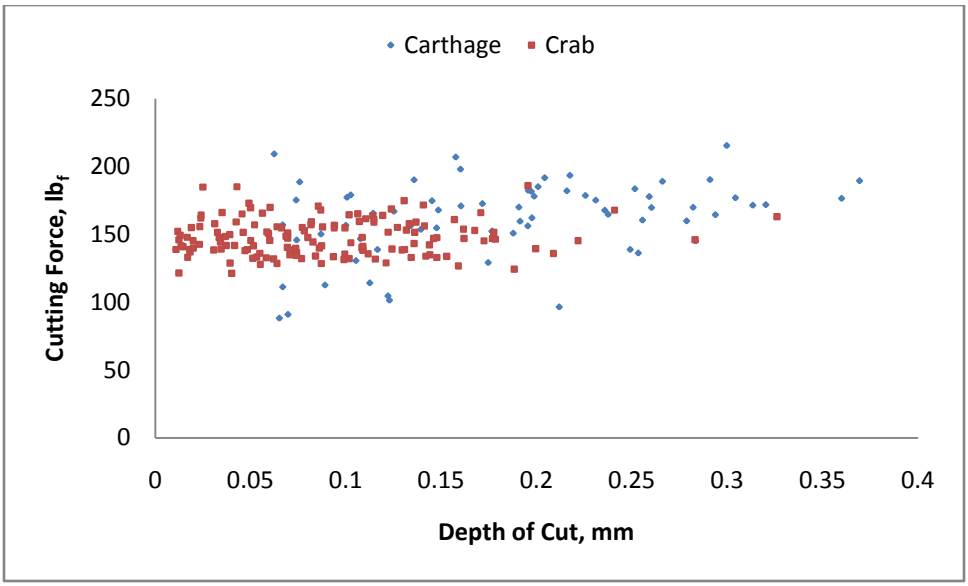

Fig. 6.18: Cutting force vs. DOC for Carthage Marble and Crab Orchard at 250 psi

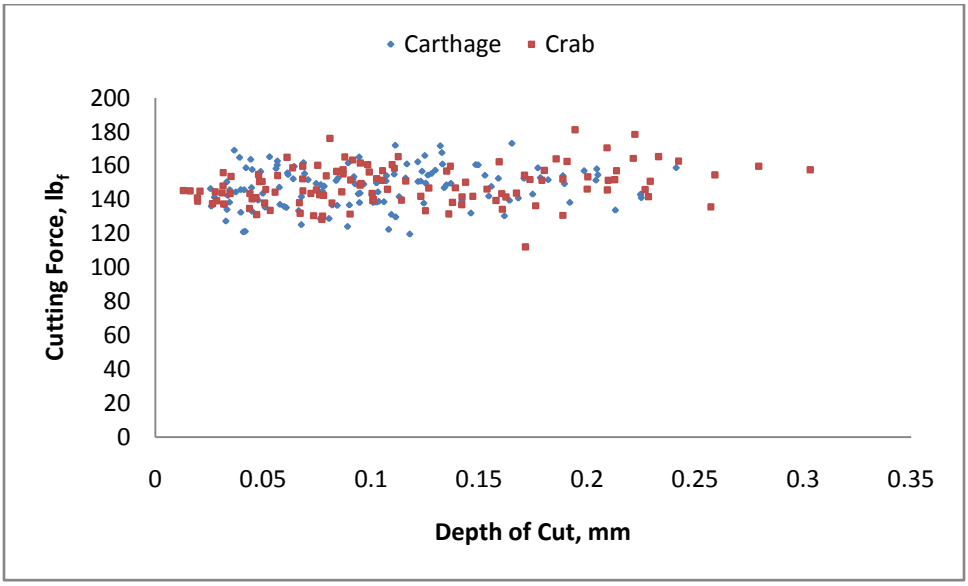

Fig. 6.19: Cutting force vs. DOC for Carthage Marble and Crab Orchard at 500 psi

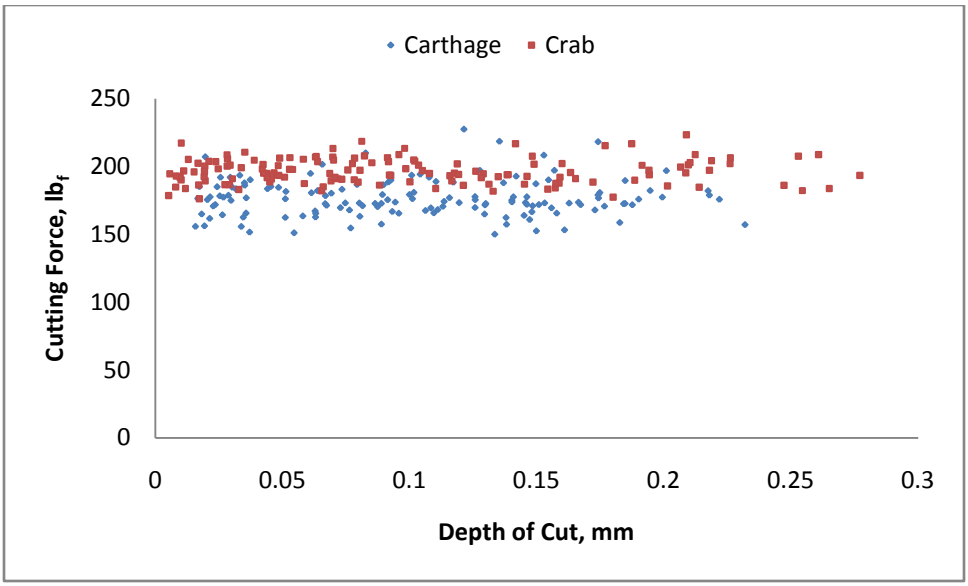

Fig. 6.20: Cutting force vs. DOC for Carthage Marble and Crab Orchard at 1,000 psi

Cutting force values for both rock types at 250 psi and 500 psi are comparable, but for Crab Orchard, a significant increase is seen at 1,000 psi. The increase of cutting force for Crab Orchard at 1,000 psi can be attributed to the fact that as the strength of the rock increases with the increase in confining pressure, the cutting force required to drill the same DOC also increases. This signifies the fact that Carthage Marble and Crab Orchard behave differently at high confining pressures.

Detournay [70], in his analysis, proposed a way to calculate pore pressure change in the shear plane. Using the same method, change in porosity during the failure of rock was determined.

Fig. 6.21 and **Fig. 6.22** show the change in porosity at the shear plane with the depth of cut for Carthage Marble and Crab Orchard respectively.

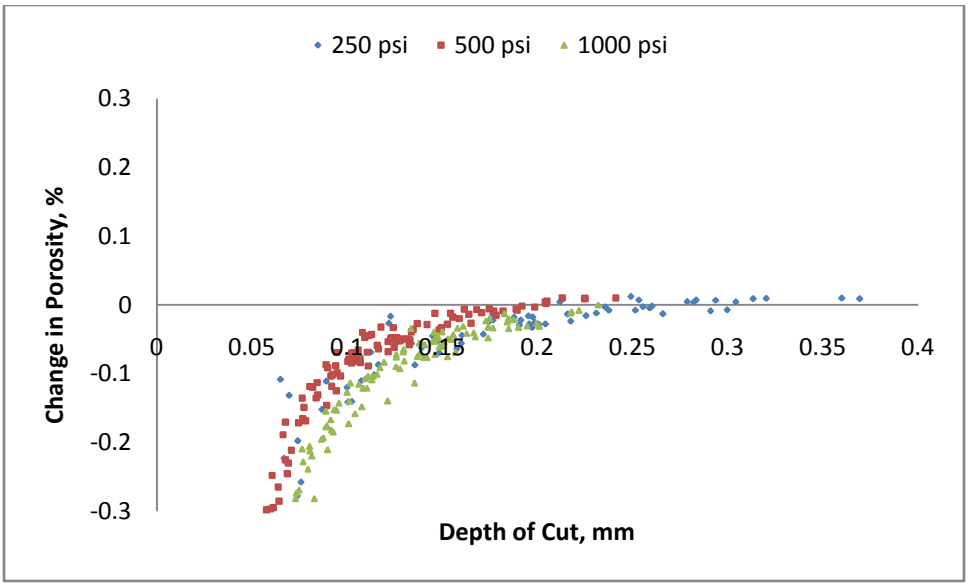

Fig. 6.21: Change in porosity with DOC in Carthage Marble at different confining pressures

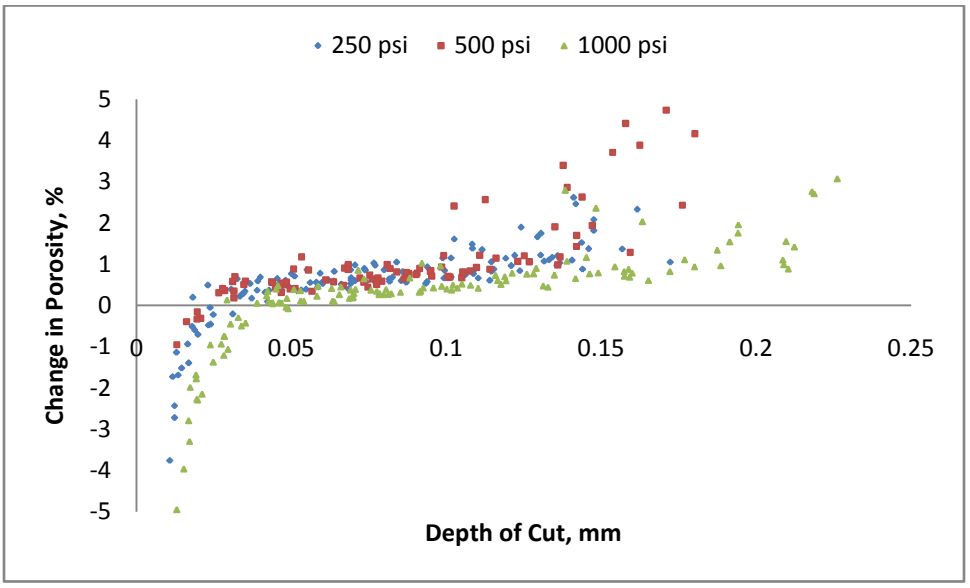

Fig. 6.22: Change in porosity with DOC in Crab Orchard at different confining pressures

Porosity change should be positive during a normal drilling process; however, Fig. 6.21 and Fig. 6.22 illustrate the process going differently.

This unexpected result prompted us to have a serious look at our cuttings collected from the drilling experiment. The dried cuttings were just like a powder, and a visual inspection was enough to note that the grains of both the rocks were destroyed in the drilling process. This behavior was not at all expected since most of the researchers have determined that the cuttings produced under external pressure are bigger in size and tend to bond together compared to the chips produced under atmospheric conditions. There seems to be a fundamental difference between atmospheric drilling and drilling under external pressure.

High values of MSE during the drilling process also support the fact that a lot of extra energy is being used somewhere else in the process. Due to the inherent structure of the set up, we don't accept that this energy is being wasted by vibrations or by frictional forces.

To get a better insight of the drilling process that causes this high value of MSE, we analyzed the cuttings from the drilling experiment under a microscope. Since the cuttings are in the form of loose particles, they are treated with epoxy to make a thin section. Thin sections are also made from the rock samples of Carthage Marble and Crab Orchard. **Fig. 6.23** and **Fig. 6.24** show different grains of Carthage Marble under a

microscope in thin sections made from Carthage Marble samples before drilling.

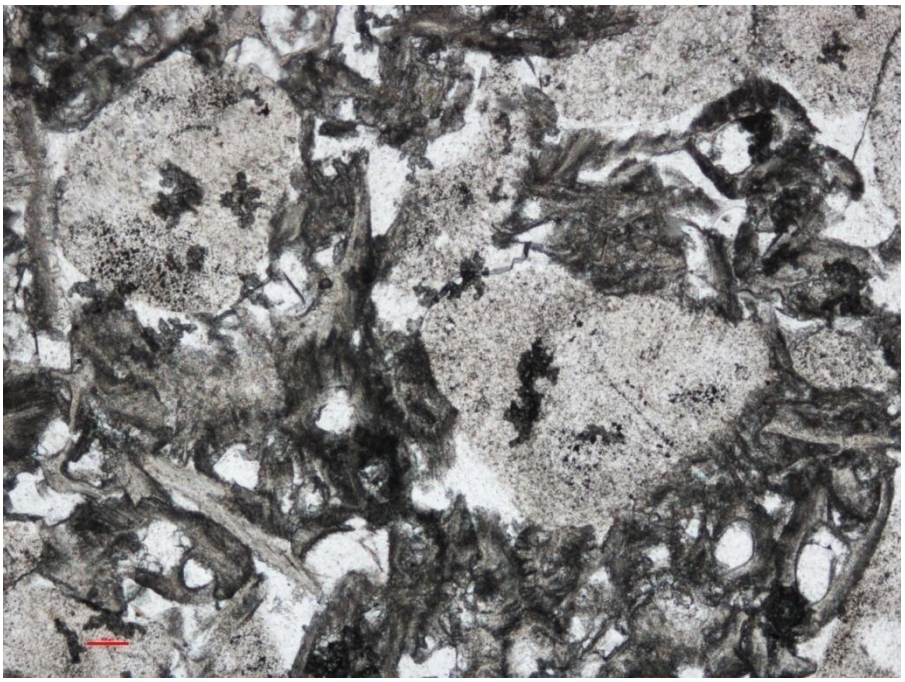

Fig. 6.23: Grains shown in a thin section of Carthage Marble

Grains of Carthage Marble can be clearly seen in the figures. The dense, black material is part of the matrix of the Carthage Marble.

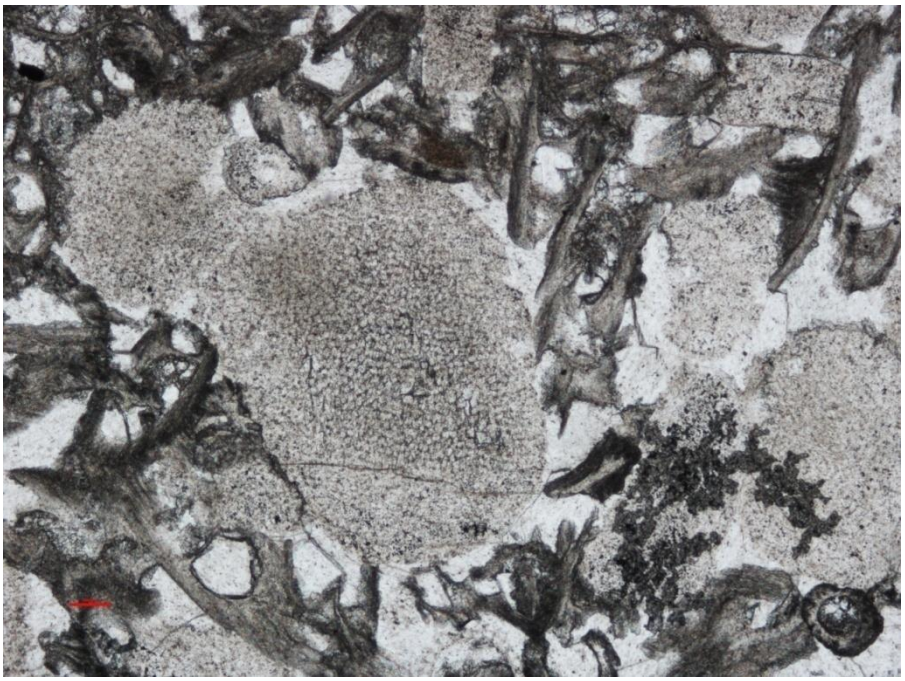

Fig. 6.24: A large size grain as seen in a thin section of Carthage Marble

Similarly, **Fig. 6.25** shows the grains of Crab Orchard under a microscope in a thin section to highlight the grain size.

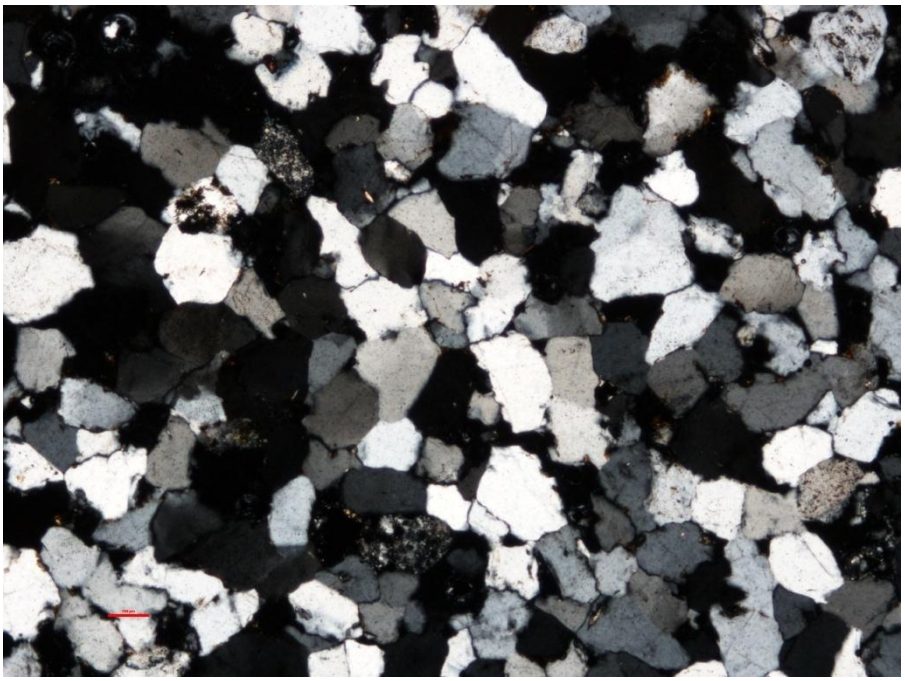

Fig. 6.25: Grains shown in a thin section of Crab Orchard

Fig. 6.26, **Fig. 6.27**, and **Fig. 6.28** show the grain size of the cuttings obtained from the experiments.

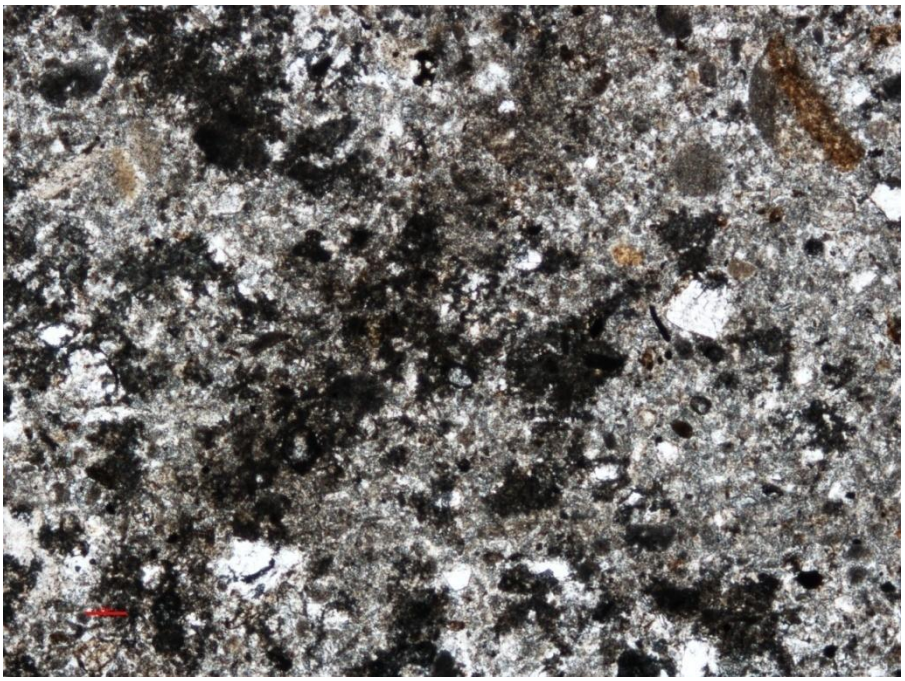

Fig. 6.26: Grains in the cuttings obtained from the drilling experiments

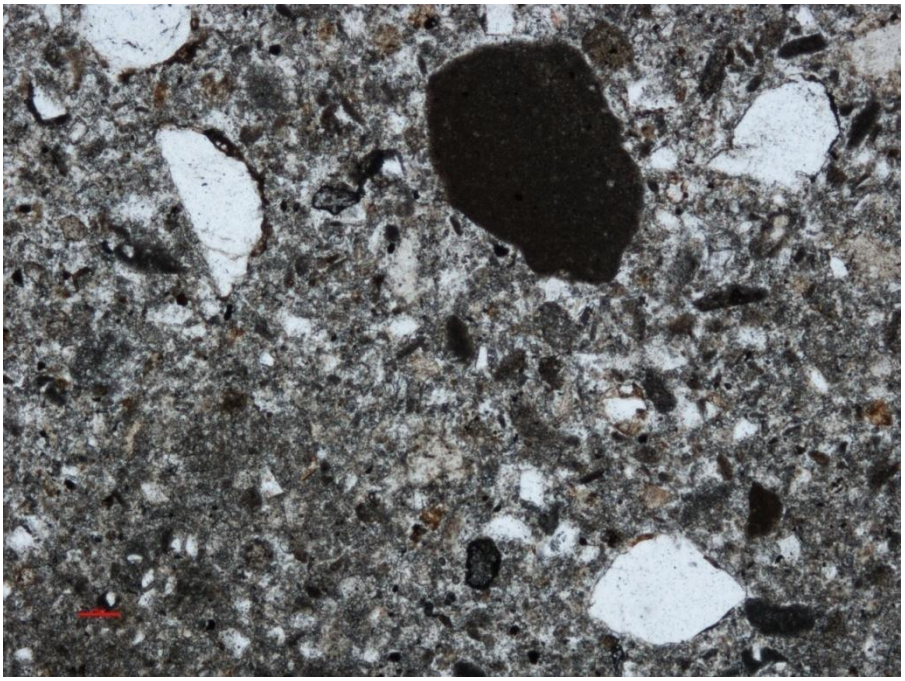

Fig. 6.27: Grains in the cuttings obtained from the drilling experiments in a different position

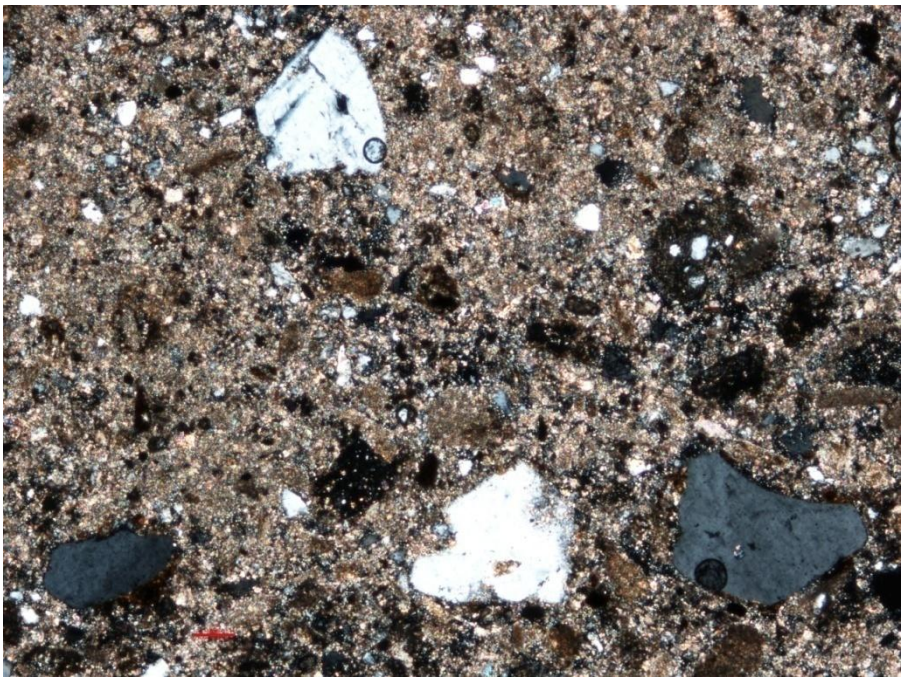

Fig. 6.28: Grains in the cuttings obtained from the drilling experiments in a different position in a different view

From the thin section results of the cuttings, it is quite clear that most of the grains were crushed or grinded during the drilling experiments. As seen in Fig. 6.26, no clear grains can be seen. However, by changing the position of the thin section, as in Fig. 6.27 and Fig. 6.28, quite a few grains can be seen. After comparing these grains from the intact rock samples in Fig. 6.23, Fig. 6.24, and Fig. 6.25, it is quite clear that most of the grains lost their shape and size due to crushing or grinding. The presence of a few half-broken grains can be explained by the grains that jumped out of the failure plane during the grinding or crushing action of the bit.

This study of thin sections of rock samples and cuttings prove that during drilling, instead of chip formation, grinding action takes place and much more energy is required for grains to be crushed in comparison to breaking bonds between grains.

In earlier work done by Rafatian et al. [80], similar observations were made. In the low range of DOC, they observed a very high value of MSE, and they offered a different perspective to this process. According to Rafatian et al. [80], under pressure and in low range of depth of cut, cutter action is more like grinding. Under pressure conditions, crushed rock accumulates in front of the cutter, which is caused by the differential pressure created due to shear dilatancy. This pile up of crushed rock apparently causes the confined strength of the crushed rock to be very high. Friction forces, observed between the grains of crushed rock, are very high and consume a large part of the energy spent in the cutting process. This friction is dependent on differential pressure and hence on dilatancy of the rock. High mechanical specific energy is required to overcome these friction forces.

CHAPTER VII

CONCLUSIONS

It is known that rocks show higher strength under high confining pressure. Drilling of hard rocks in the bottomhole is always carried out under the pressure of drilling fluid. Experiments under low confinement pressures present good insight into the drilling process and mechanical specific energy variations. The following conclusions can be summarized from the drilling experiments on Carthage Marble and Crab Orchard.

Firstly, mechanical specific energy for Carthage Marble and Crab Orchard increases with the increase in confining pressure. Crab Orchard gives higher mechanical specific energy compared to Carthage Marble in the same drilling conditions. A very high value of mechanical specific energy for both the rocks shows that the drilling process is not optimal.

Secondly, mechanical specific energy decreases with increases in depth of cut and we believe that it will get close to confined compressive strength of the rocks at optimum depth of cut. For the same depth of cut, Crab Orchard shows higher mechanical specific energy. Also, There should be a critical depth of cut at which cutting action goes from grinding to chip formation.

In Carthage Marble, the rate of penetration is high at low pressure and decreases with increase in pressure.

With an increase in depth of cut, cutting forces are found to increase in both the rock types. Required cutting force is higher at high pressure. Crab Orchard shows a significant increase in cutting force after increasing the confining pressure from 500 psi to 1,000 psi compared to increasing pressure from 250 psi to 500 psi.

Finally, investigation of cuttings show that most of the grains are crushed in the experiments and this explains very high mechanical specific energy values observed in the experiments.

CHAPTER VIII

RECOMMENDATIONS FOR FUTURE WORK

A great deal of effort was used to renovate high pressure drilling equipment and Microbit program. A conscious effort was made to utilize these equipments to the fullest to generate quality data that allows for the analysis of different variables. As with all the available facilities, a lot more can be achieved with some proper improvements to the given set up and planning of the experiments.

A more sophisticated approach to control the pore pressure, confining pressure, and mud pressure separately can provide a better insight into the different phenomenon occurring during the drilling process. I recommend upgrading the facility to control the pore pressure, confining pressure, and mud pressure separately to analyze the effect of different pressure parameters independently.

I also suggest conducting the experiments with high weight on bit since depth of cut is dependent on the weight on bit. The constraint for the weight on the bit comes from the load carrying capacity of the two rods that move the rock holder with the help of a hydraulic cylinder.

At present, the data acquisition system does not provide us with the cutting forces directly from the gauges. A direct measure of radial and

tangential force on the cutters can be utilized in a better way to differentiate drilling and grinding process during the experiments.

Finally, the study of formation of chips is an integral part of the study. A closer visual inspection during chip formation can be set up by installing high resolution, closed-circuit cameras and compatible monitors. This capability can also be used to avoid any possible failure inside the high pressure rock chamber.

REFERENCES

[1] R. Feenstra, "Status of Polycrystalline-Diamond-Compact Bits: Part I Development," *SPE Journal of Petroleum Technology,* vol. 40, pp. 675-684, 1988.

[2] B. F. Johnston, "Micromechanical Modeling of Single PDC Cutter Forces Using the Distinct Element Method," Master of Science, Department of Petroleum Engineering, Montana Tech of the University of Montana, Butte, 2003.

[3] K. K. Millheim, *et al.*, *Applied Drilling Engineering* , vol. 2. Richardson: Society of Petroleum Engineers, 1986.

[4] W. W. Olson, *et al.*, "Modeling of Chip Dynamics in Drilling," *Proceedings of CIRP International Workshop on Modeling of Machining Operations*, Atlanta, GA, pp. 347-361, 1998.

[5] A. G. Atkins, "Modelling Metal Cutting Using Modern Ductile Fracture Mechanics: Quantitative Explanations for Some Longstanding Problems," *International Journal of Mechanical Sciences,* vol. 45, pp. 373-396, 2003.

[6] V. P. Astakhov and S. Shvets, "The Assessment of Plastic Deformation in Metal Cutting," *Journal of Materials Processing Technology,* vol. 146, pp. 193-202, 2004.

[7] J. Xue*, et al.*, "Soft Rock Cutting Mechanics Model of TBM Cutter and Experimental Research," presented at the Proceedings of the 2nd International Conference on Intelligent Robotics and Applications, Singapore, 2009.

[8] I. Evans and C. D. Pomeroy, *The strength, fracture and workability of coal*: Pergamon Press, Oxford, 1966.

[9] S. U. Romero and B. B. Gomez, "Brittle and Plastic Failure of Rocks" *International Society for Rock Mechanics*, vol. 1, 1970.

[10] K. E. Gray*, et al.*, "Two-Dimensional Study of Rock Breakage in Drag-Bit Drilling at Atmospheric Pressure," *SPE Journal of Petroleum Technology,* vol. 14, pp. 93-98, 1962.

[11] D. H. Zeuch and J. T. Finger, "Rock Breakage Mechanisms With a PDC Cutter," presented at the SPE Annual Technical Conference and Exhibition, Las Vegas, Nevada, 1985.

[12] X. Wei, *et al.*, "Study of Fracture Mechanism of Rock Cutting," *Machining of Natural Stone Materials,* vol. 250, pp. 200-208, 2003.

[13] H. Guo, *et al.*, "Rock Cutting Study Using Linear Elastic Fracture Mechanics," *Engineering Fracture Mechanics,* vol. 41, pp. 771-778, 1992.

[14] H. Yotaro and C. Kenji, "Analysis Of the Mechanism of Soil : 1st Report. Cutting Patterns of Soils," *Bulletin of JSME,* vol. 18, pp. 619-626, 1975.

[15] S. A. Miedema, "Production Estimation Based on Cutting Theories for Cutting Water Saturated Sand," in WODCON IV, Amsterdam, The Netherlands, 1995.

[16] P. L. B. Oxley and M. C. Shaw, "Mechanics of Machining: An Analytical Approach to Assessing Machinability," *Journal of Applied Mechanics,* vol. 57, pp. 253-253, 1990.

[17] T. Ozel and E. Zeren, "A Methodology to Determine Work Material Flow Stress and Tool-Chip Interfacial Friction Properties by Using Analysis of Machining," *Journal of Manufacturing Science and Engineering-Transactions of the Asme,* vol. 128, pp. 119-129, 2006.

[18] Y. Nishimatsu, "The mechanics of Rock Cutting," *International Journal of Rock Mechanics and Mining Sciences & Geomechanics Abstracts,* vol. 9, pp. 261-270, 1972.

[19] J. Jonak and J. Podgórski, "Mathematical Model and Results of Rock Cutting Modeling," *Journal of Mining Science,* vol. 37, pp. 615-618, 2001.

[20] S.T. Lei and P. Kaitkay, "Distinct Element Modeling of Rock Cutting under Hydrostatic Pressure," *Key Engineering Materials,* vol. Machining of Natural Stone Materials, pp. 110-117, 2003.

[21] P. L. Menezes, *et al.*, "Finite Element Modeling of Discontinuous Chip Formation During Rock Cutting," *ASME Conference Proceedings,* vol. 2009, pp. 463-465, 2009.

[22] Y. Shenghua, "Simulation of Rock Cutting by the Finite Element Method," Available: www.ansys.com/staticassets/ANSYS/.../2004-Int-ANSYS-Conf-61.PDF

[23] G. Block and H. Jin, "Role of Failure Mode on Rock Cutting Dynamics," presented at the SPE Annual Technical Conference and Exhibition, New Orleans, Louisiana, 2009.

[24] J. F. Brett*, et al.*, "Bit Whirl - A New Theory of PDC Bit Failure," *SPE Drilling Engineering,* vol. 5, pp. 275-281, 1990.

[25] M. E. Merchant, "Mechanics of the Metal Cutting Process. I. Orthogonal Cutting and a Type 2 Chip," *Journal of Applied Physics,* vol. 16, pp. 267-275, 1945.

[26] W. J. Vlasblom, Available: http://www.dredging.org/documents/ceda/downloads/vlasblom-cutting-of-rock-may-2007.pdf

[27] V. P. Astakhov, "On the Inadequacy of the Single-Shear Plane Model of Chip Formation," *International Journal of Mechanical Sciences,* vol. 47, pp. 1649-1672, 2005.

[28] N. N. Zorev, *Metal Cutting Mechanics*. Oxford: Pergamon Press, 1966.

[29] H. L. D. Pugh, "Mechanics of Metal Cutting Process," in Proceedings of the IME conference on Technical Engineering Manufacture, London, 1958.

[30] R. E. Goodman, *Introduction to Rock Mechanics*, Second ed.: John Wiley & Sons, 1989.

[31] J. A. Franklin and M. B. Dusseault, *Rock Engineering* : McGraw-Hill, 1989.

[32] R. H. G. Parry, *Mohr Circles, Stress Paths and Geotechnics*, First ed.: E & FN Spon, 1995.

[33] J. C. Jaeger and N. G. W. Cook, *Fundamentals of Rock Mechanics*: Methuen & Co Ltd, 1969.

[34] S. A. F. Murrell, "A Criterion for Brittle Fracture of Rocks and Concrete Under Triaxial Stress, and the Effect of Pore Pressure on the Criterion," in Proceedings of Fifth Rock Mechanics Symposium in Rock mechanics, University of Minnesota, 1963.

[35] E. Hoek and E. T. Brown, "Empirical Strength Criterion for Rock Masses," *American Society of Civil Engineers,* vol. 106, pp. 1013-1035, 1980.

[36] R. K. Yudhbir, *et al.*, "An Empirical Failure Criterion for Rock Masses," in Proceedings of the 5th International Congress on Rock Mechanics, vol. 1, pp. 1-8, 1983.

[37] I. W. Johnston, "Strength of Intact Geomechanical Materials," *Journal of Geotechnical Engineering-Asce,* vol. 111, pp. 730-749, 1985.

[38] L. Zhang, *Engineering Properties of Rocks*, vol. 4: Elsevier, 2005.

[39] A. B. Hawkins and B. J. McConnell, "Sensitivity of Sandstone Strength and Deformability to Changes in Moisture Content," *Quarterly Journal of Engineering Geology and Hydrogeology,* vol. 25, pp. 115-130, 1992.

[40] S. A. F. Murrell, "The Effect of Triaxial Stress Systems on the Strength of Rocks at Atmospheric Temperatures," *Geophysical Journal of the Royal Astronomical Society,* vol. 10, pp. 231-281, 1965.

[41] D. W. Hobbs, "A Study of the Behaviour of a Broken Rock Under Triaxial Compression, and Its Application to Mine Roadways," *International Journal of Rock Mechanics and Mining Sciences & Geomechanics Abstracts,* vol. 3, pp. 11-43, 1966.

[42] F. D. Patton, "Multiple Modes of Shear Failure in Rock," presented at the Congress of International Society for Rock Mechanics, Lisbon, 1966.

[43] J. D. Byerlee, "Theory of Friction Based on Brittle Fracture," *Journal of Applied Physics,* vol. 38, pp. 2928-2934, 1967.

[44] J. Jonak, "Influence of Friction on the Chip Size in Cutting the Brittle Materials," *Journal of Mining Science,* vol. 37, pp. 407-410, 2001.

[45] *Rock Mechanics in Engineering Practice*: John Wiley & Sons, 1968.

[46] P. A. Charlez, *Rock Mechanics: Petroleum Applications* vol. 2: Editions Technip, 1997.

[47] S. Lei and P. Kaitkay, "Micromechanical Modeling of Rock Cutting Under Pressure Boundary Conditions Using Distinct Element Method," *Transactions of the North American Manufacturing Research Institute of SME*, vol. 30, pp. 207-214, 2002.

[48] P. Kaitkay and S. Lei, "Experimental study of rock cutting under external hydrostatic pressure," *Journal of Materials Processing Technology,* vol. 159, pp. 206-213, 2005.

[49] A. S. Murray and R. A. Cunningham, "Effect of Mud Column Pressure on Drilling Rates," *Petroleum Transactions, AIME*, vol. 204, pp. 196-204, 1955.

[50] R. A. Cunningham and J. G. Eenink, "Laboratory Study of Effect of Overburden, Formation and Mud Column Pressures on Drilling Rate of Permeable Formations," *Petroleum Transactions, AIME,* vol. 217, pp. 9-17, 1959.

[51] W. C. Maurer, "Bit - Tooth Penetration Under Simulated Borehole Conditions," *SPE Journal of Petroleum Technology,* vol. 17, pp. 1433-1442, 1965.

[52] N. E. Garner, "Cutting Action of a Single Diamond Under Simulated Borehole Conditions," *SPE Journal of Petroleum Technology,* vol. 19, pp. 937-942, 1967.

[53] D. J. Vidrine and E. J. Benit, "Field Verification of the Effect of Differential Pressure on Drilling Rate," *SPE Journal of Petroleum Technology,* vol. 20, pp. 676-682, 1968.

[54] A. J. Garnier and N. H. Van Lingen, "Phenomena Affecting Drilling Rates at Depth," *Petroleum Transactions, AIME,* vol. 216, pp. 232-239, 1959.

[55] N. H. Van Lingen, "Bottom Scavenging - A Major Factor Governing Penetration Rates at Depth," *SPE Journal of Petroleum Technology,* vol. 14, pp. 187-196, 1962.

[56] R. Feenstra and J. J. M. Van Leeuwen, "Full-Scale Experiments on Jets in Impermeable Rock Drilling," *SPE Journal of Petroleum Technology,* vol. 16, pp. 329-336, 1964.

[57] T. M. Warren and M. B. Smith, "Bottomhole Stress Factors Affecting Drilling Rate at Depth," *SPE Journal of Petroleum Technology,* vol. 37, pp. 1523-1533, 1985.

[58] D. H. Zijsling, "Single Cutter Testing - A Key for PDC Development," presented at the Offshore Europe, Aberdeen, United Kingdom, 1987.

[59] D. Gray-Stephens*, et al.*, "Influence of Pore Pressure on Drilling Response in Hard Shales," *SPE Drilling & Completion,* vol. 9, pp. 263-270, 1994.

[60] U. Prasad, "Drillability of a Rock in Terms of Its Physico-Mechanical and Micro-Structural Properties," presented at the 43rd U.S. Rock Mechanics Symposium & 4th U.S. - Canada Rock Mechanics Symposium, Asheville, North Carolina, 2009.

[61] R. Simon, "Energy Balance in Rock Drilling," *SPE Journal,* vol. 3, pp. 298-306, 1963.

[62] R. Teale, "The concept of Specific Energy in Rock Drilling," *International Journal of Rock Mechanics and Mining Sciences & Geomechanics Abstracts,* vol. 2, pp. 57-73, 1965.

[63] D. J. Reddish and E. Yasar, "A New Portable Rock Strength Index Test Based on Specific Energy of Drilling," *International Journal of Rock Mechanics and Mining Sciences & Geomechanics Abstracts,* vol. 33, pp. 543-548, 1996.

[64] D. Curry*, et al.*, "Technical Limit Specific Energy - An Index to Facilitate Drilling Performance Evaluation," presented at the SPE/IADC Drilling Conference, Amsterdam, Netherlands, 2005.

[65] E. Detournay and C. P. Tan, "Dependence of Drilling Specific Energy on Bottom-Hole Pressure in Shales," presented at the SPE/ISRM Rock Mechanics Conference, Irving, Texas, 2002.

[66] A. D. Black*, et al.*, "Effects of Pore Pressure and Mud Filtration on Drilling Rates in a Permeable Sandstone," *SPE Journal of Petroleum Technology,* vol. 37, pp. 1671-1681, 1985.

[67] R. C. Pessier and M. J. Fear, "Quantifying Common Drilling Problems With Mechanical Specific Energy and a Bit-Specific Coefficient of Sliding Friction," presented at the SPE Annual Technical Conference and Exhibition, Washington, D.C., 1992.

[68] H. U. Caicedo*, et al.*, "Unique ROP Predictor Using Bit-specific Coefficient of Sliding Friction and Mechanical Efficiency as a Function of Confined Compressive Strength Impacts Drilling Performance," presented at the SPE/IADC Drilling Conference, Amsterdam, Netherlands, 2005.

[69] E. Detournay and C. Atkinson, "Influence of Pore Pressure On the Drilling Response of PDC Bits," presented at the The 32nd U.S. Symposium on Rock Mechanics (USRMS), Norman, Oklahoma, 1991.

[70] E. Detournay and C. Atkinson, "Influence of Pore Pressure on the Drilling Response in Low-Permeability Shear-Dilatant Rocks," *International Journal of Rock Mechanics and Mining Sciences,* vol. 37, pp. 1091-1101, 2000.

[71] J. J. Kolle, "The Effects of Pressure and Rotary Speed on the Drag Bit Drilling Strength of Deep Formations," presented at the SPE Annual Technical Conference and Exhibition, Denver, Colorado, 1996.

[72] A. Judzis*, et al.*, "Optimization of Deep-Drilling Performance: Benchmark Testing Drives ROP Improvements for Bits and Drilling Fluids," presented at the SPE/IADC Drilling Conference, Amsterdam, The Netherlands, 2007.

[73] R. J. Waughman*, et al.*, "Real-Time Specific Energy Monitoring Reveals Drilling Inefficiency and Enhances the Understanding of When to Pull Worn PDC Bits," presented at the IADC/SPE Drilling Conference, Dallas, Texas, 2002.

[74] F. E. Dupriest, "Comprehensive Drill Rate Management Process To Maximize ROP," presented at the SPE Annual Technical Conference and Exhibition, San Antonio, Texas, USA, 2006.

[75] F. E. Dupriest and W. L. Koederitz, "Maximizing Drill Rates with Real-Time Surveillance of Mechanical Specific Energy," presented at the SPE/IADC Drilling Conference, Amsterdam, The Netherlands, 2005.

[76] H. Rabia, "Specific Energy as a Criterion for Bit Selection," *SPE Journal of Petroleum Technology,* vol. 37, pp. 1225-1229, 1985.

[77] P. L. Moore, *Drilling Practices Manual*. Tulsa: Penn Well Books, 1974.

[78] H. Abdollahi, *et al.*, "Drilling Optimization Using Minimum Energy Concept," presented at the 2nd Iranian Rock Mechanics Conference, Tehran, 2004.

[79] *Microbit Lab Manual*.

[80] N. Rafatian, *et al.*, "Experimental Study of MSE of a Single PDC Cutter Under Simulated Pressurized Conditions," presented at the SPE/IADC Drilling Conference and Exhibition, Amsterdam, The Netherlands, 2009.